TITLE

Keratinocyte-intrinsic BCL10/MALT1 activity initiates and amplifies psoriasiform skin inflammation

AUTHORS

Zsuzsanna Kurgyis[1,2], Larsen Vornholz[1,2], Konstanze Pechloff[1,2], Lajos V. Kemény[3], Tim Wartewig[1,2], Andreas Muschaweckh[4], Abhinav Joshi[1,2], Katja Kranen[5], Lara Hartjes[1,2], Sigrid Möckel[5,6], Katja Steiger[7], Erik Hameister[1,2], Thomas Volz[5], Mark Mellett[8], Lars E. French[8,9,10], Tilo Biedermann[5], Thomas Korn[4,11,12] & Jürgen Ruland[1,2,13,14,*]

AFFILIATIONS

[1]*Institute of Clinical Chemistry and Pathobiochemistry, School of Medicine, Technical University of Munich; Munich, Germany.*

[2]*TranslaTUM, Center for Translational Cancer Research, Technical University of Munich; Munich, Germany.*

[3]*Cutaneous Biology Research Center, Department of Dermatology and MGH Cancer Center, Massachusetts General Hospital, Harvard Medical School; Boston, MA, United States.*

[4]*Department of Experimental Neuroimmunology, Klinikum rechts der Isar, Technical University of Munich; Munich, Germany.*

[5]*Department of Dermatology and Allergy, Technical University of Munich; Munich, Germany.*

[6]*Institute of Pathology, Universität Würzburg; Würzburg, Germany.*

[7]*Institute of Pathology, School of Medicine, Technical University of Munich; Munich, Germany*

[8]*Department of Dermatology, University Hospital of Zürich, University of Zurich (UZH); Zürich, Switzerland*

[9]*Department of Dermatology and Allergy, University Hospital, LMU Munich; Munich, Germany*

[10]*Dr. Phillip Frost Department of Dermatology and Cutaneous Surgery, University of Miami Miller School of Medicine; Miami, FL*

[11]*Department of Neurology, Klinikum rechts der Isar, Technical University of Munich; Munich, Germany*

[12]*Munich Cluster for Systems Neurology (SyNergy); Munich, Germany*

[13]*German Cancer Consortium (DKTK); Heidelberg, Germany.*

[14]*German Center for Infection Research (DZIF), Munich partner site; Munich, Germany.*

*Corresponding author. Email: j.ruland@tum.de

ONE SENTENCE SUMMARY

Keratinocyte-intrinsic BCL10/MALT1 signaling can act as critical initiator and crucial amplifier of skin inflammation in murine models and is altered in human sporadic psoriasis.

ABSTRACT

Psoriasis is a chronic inflammatory skin disease arising from ill-defined pathological crosstalk between keratinocytes and the immune system. BCL10 and MALT1 are ubiquitously expressed inflammatory signaling proteins that can interact with the psoriasis susceptibility factor CARD14, but their functions in psoriasis are insufficiently understood. We report that although keratinocyte-intrinsic BCL10/MALT1 deletions completely rescue inflammatory skin pathology triggered by germline *Card14* gain-of-function mutation in mice, the BCL10/MALT1 signalosome is surprisingly not involved in the CARD14-dependent IL-17R proximal pathway. Instead, it plays a more pleiotropic role by amplifying keratinocyte responses to a series of inflammatory cytokines, including IL-17A, IL-1β and TNF. Moreover, selective keratinocyte-intrinsic activation of BCL10/MALT1 signaling with an artificial engager molecule is sufficient to initiate lymphocyte-mediated psoriasiform skin inflammation, and aberrant BCL10/MALT1 activity is frequently detected in the skin of human sporadic psoriasis. Together, these results establish that BCL10/MALT1 signalosomes can act as initiators and crucial amplifiers of psoriatic skin inflammation and indicate a critical function for this complex in sporadic psoriasis.

INTRODUCTION

Psoriasis is a chronic inflammatory skin disease that affects 2-3% of the general population *(1)*. Debilitating skin lesions and associated systemic comorbidities severely impair patient quality of life *(2)*. Histopathologically, the scaling and itching skin of psoriasis patients is characterized by hyperproliferative keratinocytes and mixed inflammatory infiltrates that mainly consist of lymphocytes and neutrophil granulocytes. While the pathological interplay between keratinocytes and the innate and adaptive immune systems is known to drive pathogenesis, the underlying mechanisms have been insufficiently defined.

In most cases, psoriasis is based on a complex genetic trait; therefore, several genome-wide association studies (GWAS) have been performed *(3–6)*. These studies have revealed that a large number of psoriasis susceptibility genes are linked to the inflammatory NF-κB pathway (e.g., *CARD14, NFKBIA, NFKBIZ, REL, TNFAIP3 and TNIP1)* or directly to the IL-23/Th17 signaling axis (e.g., *IL12B, IL23A, IL23R*, *JAK2, STAT3, TRAF3IP2 and TYK2*). Individually, most of these risk factors confer only a low risk of disease development (odds ratio < 1.5). However, caspase recruitment domain family member 14 *(CARD14,* also known as *CARMA2*) has not only been linked to *psoriasis susceptibility locus 2* (PSORS2) by GWAS but has also been causally connected to rare forms of familial psoriasis *(7–10)* and the related inflammatory skin disease pityriasis rubra pilaris *(11–13)*, indicating that it controls particularly important pathways for these disorders.

CARD14 (or CARMA2) is a proinflammatory signaling molecule that is physiologically expressed in several cell types in the skin, including keratinocytes *(7)*, Langerhans cells *(14)*, dermal γδ T cells *(14)* and endothelial cells *(15)*, and in the placenta *(16)* and gut *(11)*. This

molecule contains an N-terminal caspase recruitment domain (CARD), a central coiled-coil (CC) and linker domain, and a C-terminal MAGUK region *(17)*. Psoriasis-associated gain-of-function (GOF) mutations result in structural alterations within CARD14 that disrupt intramolecular autoinhibition and lead to constitutive activation of the NF-κB pathway *in vitro* and *in vivo (18, 19)*. Recently developed knock-in mouse models that possess psoriasis-associated *Card14* mutations in their germline or in keratinocytes develop psoriasiform skin inflammation with histopathological features of human psoriasis, demonstrating that these alterations are sufficient to drive pathology *(19–22)*. In this context, it has been demonstrated that CARD14 acts proximally at the IL-17 receptor (IL-17R) and links IL-17R ligation to activation of the canonical IκB kinase-(IKK)-induced NF-κB signaling pathway via a direct interaction with the ubiquitin ligase TRAF6 and the adapter protein ACT1 *(21)*, which has been suggested to explain the pathogenic role of *CARD14-GOF* alterations in inherited skin inflammation *(21, 23)*.

In addition to interacting with TRAF6 and ACT1, CARD14 also binds via its CARD domain to the CARD of the adaptor molecule BCL10 *(16–18, 24–26)*, which constitutively interacts with the paracaspase MALT1 *(17)*. BCL10 and MALT1 form ubiquitously expressed signalosomes, which can be activated by a large series of upstream stimuli in different cell types *(17)*, including antigen receptor signals in lymphocytes, microbial signals via pattern recognition receptors such as Dectin-1 or via receptor tyrosine kinases and G-protein coupled receptors in innate immune cells and in nonhematopoietic tissues, including the skin *(17)*. Activation of the BCL10/MALT1 signaling module triggers IKK-mediated NF-κB signaling as well as the p38 and JNK kinase cascades *(17)*. In addition, MALT1 functions as a cysteine protease that can cleave an array of inflammatory regulators to provide an additional layer of context-specific gene expression control *(17)*. Although psoriasis-associated CARD14-GOF variants can constitutively assemble

98 and activate the BCL10/MALT1 module *(18, 19)*, the molecular and cellular functions of this
99 signalosome in the complex pathogenesis of psoriasis are insufficiently defined.

100 To explore the roles of BCL10 and MALT1 in inflammatory skin disease, we engineered
101 a series of conditional mouse mutants to specifically activate, inactivate or attenuate
102 BCL10/MALT1 signaling in keratinocytes *in vivo*. We report that while keratinocyte-intrinsic
103 BCL10/MALT1 complexes are absolutely critical for skin inflammation triggered by germline
104 *Card14-GOF* mutations, the BCL10/MALT1 complex is surprisingly not involved in IL-17R
105 proximal events. Instead, it amplifies keratinocyte responses to multiple proinflammatory
106 cytokines. In addition, keratinocyte-intrinsic activation of BCL10/MALT1 signaling alone is
107 sufficient to drive psoriasiform skin inflammation *in vivo,* and altered BCL10/MALT1 signaling
108 is frequently detected in human sporadic psoriasis.

RESULTS

Keratinocyte-intrinsic BCL10/MALT1 signaling mediates *Card14$^{\Delta E138}$*- and chemically induced skin inflammation

Knock-in mice with a psoriasis-associated germline mutation in the *Card14* locus spontaneously develop chronic skin inflammation with features of human psoriasis *(19–21)*. Since CARD14 is expressed in several cell types *(7, 11, 14, 15)*, we first explored the keratinocyte-intrinsic functions of BCL10 and MALT1 in *Card14$^{\Delta E138}$* mice by crossing these animals to mice that harbor homozygous conditional *Bcl10 (27)* or *Malt1 (27)* alleles and a keratinocyte-specific *Cre* driven by the *Keratin14* promoter *(Bcl10$^{KC\text{-}KO}$* and *Malt1$^{KC\text{-}KO}$) (28)*. Compound mutant mice harbor a *Card14$^{\Delta E138}$* GOF allele in all cell types and keratinocyte-specific deletions of either the *Bcl10* (*Card14$^{\Delta E138}$;Bcl10$^{KC\text{-}KO}$*) (**Fig. 1A** for schematic) or *Malt1* locus (*Card14$^{\Delta E138}$;Malt1$^{KC\text{-}KO}$*). Intriguingly, keratinocyte-specific deletion of either *Bcl10* or *Malt1* completely rescued the chronic skin inflammation driven by *Card14$^{\Delta E138}$*, as *Card14$^{\Delta E138}$;Bcl10$^{KC\text{-}KO}$* and *Card14$^{\Delta E138}$;Malt1$^{KC\text{-}KO}$* mice displayed no macroscopic signs of inflammation (**Fig. S1A-B**), and the characteristic ear thickening of *Card14$^{\Delta E138}$* animals was also absent (**Fig. 1B-C**). The histological analysis of *Card14$^{\Delta E138}$* mice showed in the presence of BCL10 and MALT1 an acanthotic epidermis with focal hypogranulosis and mounds of parakeratosis housing neutrophils, dilated capillaries and a perivascular infiltrate with lymphocytes and neutrophils characteristic of psoriasiform skin inflammation. All these pathological features were completely absent in the skin of *Card14$^{\Delta E138}$;Bcl10$^{KC\text{-}KO}$* and *Card14$^{\Delta E138}$;Malt1$^{KC\text{-}KO}$* animals (**Fig. 1D-E**).

Flow cytometric analysis confirmed the increased numbers of skin-infiltrating neutrophil granulocytes and αβ T cells, including those expressing IL-17A, in *Card14$^{\Delta E138}$* mice, while γδ T

cell counts were normal. These pathological infiltrates were also not detected upon keratinocyte-intrinsic *Bcl10* or *Malt1* deletion (**Fig. 1F-K** and **Fig. S1C-F**). In addition, the IL-17 target genes *Cxcl1*, *Csf2, S100a8*, *Lcn2* and *Tnf* were elevated in the skin of $Card14^{\Delta E138}$ mice but not in the skin of $Card14^{\Delta E138};Bcl10^{KC\text{-}KO}$ and $Card14^{\Delta E138};Malt1^{KC\text{-}KO}$ animals (**Fig. S1G-P**). Together, these results establish at the genetic level that keratinocyte-intrinsic activation of BCL10/MALT1 signaling is absolutely critical for psoriasiform skin inflammation triggered by a germline *Card14-GOF* mutation.

To study the role of keratinocyte-intrinsic BCL10/MALT1 signalosomes in an alternative and well-established murine model of psoriasis, we next utilized $Bcl10^{KC\text{-}KO}$ mice and treated them with the imiquimod-containing cream Aldara *(29)*. Imiquimod is a TLR7/9 agonist that induces IL-17A-dependent psoriasis-like skin inflammation *(29)*. The daily topical application of imiquimod to the back and ears of wild-type mice led, as expected, to strong skin inflammation with local swelling (**Fig. 1L-M**), the infiltration of neutrophils as well as αβ T cells and IL-17A-expressing αβ T cells (**Fig. 1N-P**) and the expression of various cytokines and chemokines, such as *Cxcl1, Lcn2, S100a8* and *S100a9* (**Fig. 1Q-T**), as previously described *(29)*. In the absence of keratinocyte-intrinsic BCL10, this inflammatory response was significantly reduced however did not abate the signal completely (Fig. 1L-T).

BCL10/MALT1 activation in keratinocytes drives psoriasiform skin inflammation

After establishing a keratinocyte-intrinsic requirement of BCL10/MALT1 signaling complexes in genetic and chemically induced skin inflammation, we next were interested in whether selectively enforced activation of BCL10/MALT1 signaling only within keratinocytes

would be sufficient to trigger pathology. To explore this question in the absence of CARD14-GOF, which could have additional effects, such as in the IL-17R proximal pathway *(21)*, we engineered an experimental BCL10/MALT1 engager molecule based on the protein CARD11, which is normally mostly expressed in lymphocytes in addition to mast cells and in the skin *(17, 30, 31)*. To create a constitutively active form of CARD11, we deleted the autoinhibitory CARD-MAGUK linker domain *(32)* and termed this BCL10/MALT1 activator CARD11$^{\Delta Linker}$. To engage BCL10/MALT1 signalosomes in a cell-type specific manner *in vivo*, we next introduced *Card11$^{\Delta Linker}$* cDNA together with GFP cDNA, preceded by a loxP-flanked STOP cassette, in the ubiquitously expressed *Rosa26* locus (**Fig. S2A-B**). For keratinocyte-specific expression, we crossed these animals with *K14Cre* mice (**Fig. 2A** for schematic). In the offspring (*Card11$^{\Delta Linker\text{-}KC}$* mice), we detected keratinocyte-intrinsic expression of CARD11$^{\Delta Linker}$ (**Fig. S2C**).

Intriguingly, all *Card11$^{\Delta Linker\text{-}KC}$* mice developed an inflammatory skin disorder characterized by scaling, thickening and redness of the ears with 100% penetrance (**Fig. 2B**). Keratinocytes isolated from *Card11$^{\Delta Linker\text{-}KC}$* mice exhibited increased NF-κB activity (**Fig. 2C**) and cell-autonomous inflammatory gene expression without exogenous stimulation (**Fig. 2D**). Crosses of *Card11$^{\Delta Linker\text{-}KC}$* mice to *Bcl10$^{KC\text{-}KO}$* or *Malt1$^{KC\text{-}KO}$* mice completely rescued the phenotype (**Fig. 2E**), demonstrating that the keratinocyte-intrinsic activation of BCL10/MALT1 signaling was indeed responsible for driving this disease. Histopathological analysis of *Card11$^{\Delta Linker\text{-}KC}$* mice demonstrated acanthosis, lymphocytic and neutrophil granulocytic infiltration and increased vascularization, which are classical characteristics of psoriasis (**Fig. 2F-G**). Quantification of the histological signs observed in *K14Cre;Card11$^{\Delta Linker}$* mice using the psoriasis histology score developed by Baker et al. *(33)* confirmed the resemblance to psoriatic

lesions (Fig. 2F), which were completely absent in animals lacking either keratinocyte BCL10 or MALT1 (Fig. 2G).

Similar to psoriasis patients, *Card11*$^{\Delta Linker\text{-}KC}$ animals showed increased numbers of neutrophil granulocytes in the skin (**Fig. 3A** and **Fig. S3A**) as well as αβ T cells (**Fig. 3B** and **Fig. S3B**), while dermal γδ T cell counts were comparable to those in control littermates (**Fig. S3B-C**). In particular, IL-17A-producing αβ T cells were expanded (**Fig. 3C**), while the numbers of IL-17A+ γδ T cells were not increased (**Fig. S3D**). Moreover, mRNA expression analyses of the inflamed skin tissue revealed the upregulation of *Il17a* transcripts (**Fig. 3D**), whereas the expression of the Th1 and Th2 signature cytokines *Ifng* and *Il4* was not increased in *Card11*$^{\Delta Linker\text{-}KC}$ animals (**Fig. 3E-F**). We also found increased expression of *Ccl20* (**Fig. 3G**), a major chemokine attracting CCR6+ and IL-17A-expressing T cells *(34)*, which might explain their high numbers in the skin. In line with enhanced IL-17A-mediated pathology, the IL-17 target genes *Cxcl1* and *Cxcl5* as well as *Csf2* were also upregulated in the inflamed skins of *Card11*$^{\Delta Linker\text{-}KC}$ mice (**Fig. 3H**), which likely explains the high numbers of infiltrating granulocytes. Additional IL-17 target genes, such as *S100a8*, *Lcn2*, and *Tnf,* were also upregulated in *Card11*$^{\Delta Linker\text{-}KC}$ skins (Fig. 3H). Again, the expression of IL-17 target genes was not enhanced in *Card11*$^{\Delta Linker\text{-}KC}$*;Bcl10*$^{KC\text{-}KO}$ and *Card11*$^{\Delta Linker\text{-}KC}$*;Malt1*$^{KC\text{-}KO}$ mice (**Fig. S3E-F**). Furthermore, treatment of *Card11*$^{\Delta Linker\text{-}KC}$ animals with anti-IL-17A significantly decreased the skin thickness (**Fig. 3I**) and reduced neutrophil granulocyte numbers to wild-type levels (**Fig. 3J**). Thus, keratinocyte-intrinsic activation of the BCL10/MALT1 signalosome by CARD11$^{\Delta Linker}$ drives Th17-dominated psoriasiform skin inflammation with key characteristics of human psoriasis.

Enforced BCL10/MALT1 signaling in keratinocytes triggers lymphocyte-mediated pathology

To understand the mechanisms of keratinocyte-intrinsic CARD11$^{\Delta Linker}$/BCL10/MALT1-induced skin inflammation and to specifically explore the role of lymphocytes in this pathology, we next crossed *Card11$^{\Delta Linker\text{-}KC}$* mice with *Rag2*-deficient animals that lack T and B cells *(35)*. Interestingly, although *Card11$^{\Delta Linker\text{-}KC}$;Rag2$^{-/-}$* mice showed increased epidermal thickening and keratinization (**Fig. 4A**) with an upregulation of the keratinocyte activation and proliferation markers *Krt6* and *Krt16* (**Fig. 4B**) *(36, 37)*, expression of the Th17 target genes *Cxcl1, Cxcl5, Csf2, Lcn2* and *Tnf* was, in contrast to *Card11$^{\Delta Linker\text{-}KC}$* mice, not increased in *Card11$^{\Delta Linker\text{-}KC}$;Rag2$^{-/-}$* animals (**Fig. 4C**). Moreover, although some ear swelling was detectable, most likely due to epidermal changes, their ear thickness was greatly reduced in comparison to that of *Card11$^{\Delta Linker\text{-}KC}$* mice (**Fig. 4D**), and the strong neutrophilic infiltration seen in the skin of *Card11$^{\Delta Linker\text{-}KC}$* mice was not observed in *Card11$^{\Delta Linker\text{-}KC}$;Rag2$^{-/-}$* animals (**Fig. 4E**). Thus, although keratinocyte-intrinsic CARD11$^{\Delta Linker}$ signaling can drive keratinocyte activation and hyperkeratosis, the presence of lymphocytes is necessary to induce full psoriasiform pathology.

BCL10/MALT1 signaling in keratinocytes amplifies secondary cytokine circuits

In psoriasis, lymphocyte-derived cytokines can stimulate keratinocytes, which then amplify inflammation *(38)*. To test the keratinocyte-intrinsic roles of BCL10 and MALT1 in secondary cytokine-induced keratinocyte responses, we isolated keratinocytes from *Bcl10$^{-/-}$ (39)* or *Malt1$^{-/-}$* mice *(40)* and stimulated them with psoriasis-related and lymphocyte-derived factors IL-17A, IL-1β or TNF (**Fig. 5A** for schematic). In the absence of BCL10, IL-17A, IL-1β and TNF

were unable to induce the regular expression of their target genes *Tnf*, *Cxcl5* and *Csf2* (**Fig. 5B-E**). Likewise, *Malt1*-deficient keratinocytes *(40)* were also substantially impaired in inducing *Tnf*, *Cxcl5* and *Csf2* expression upon IL-17A or IL-1β stimulation (**Fig. 5F-I**). In contrast, *Card11*$^{\Delta Linker\text{-}KC}$ keratinocytes with activated BCL10/MALT1 signaling exhibited substantial increases in the levels of *Tnf*, *Cxcl5* and *Csf2* production in response to IL-17A or IL-1β stimulation (**Fig. S4A-C**). Thus, while the enforced activation of the BCL10/MALT1 signalosome in keratinocytes can amplify inflammatory responses to several cytokines, the presence of endogenous BCL10 and MALT1 is essential for the normal keratinocyte response to IL-17A and IL-1β or TNF. This effect is not due to altered cytokine receptor expression, since *Bcl10*-deficient keratinocytes had normal *Il17ra*, *Tnfrsf1* and *Il1r* expression (**Fig. S4D-F**) and the surface expression of the IL-17R was also unaltered (**Fig. S4G**). Furthermore, *Bcl10*- or *Malt1*-deficient keratinocytes were not completely unresponsive to exogenous stimuli, as the IL-17A, IL-1β and TNF-induced expression of *Nfkbiz* (encoding IκBζ), which is a gene also linked to psoriasis pathogenesis *(41, 42)*, was unaffected in the absence of BCL10 or MALT1 signaling (**Fig. S4H-I**). The regulatory function of the BCL10/MALT1 signalosome in keratinocytes appears to be conserved between mice and humans, as the siRNA-mediated knockdown of *BCL10,* or *CARD14* in primary human keratinocytes also decreased IL-17A-induced *TNF, CXCL5* and *CSF2* expression (**Fig. 5J-M**).

BCL10/MALT1 signalosomes in keratinocytes release specific negative regulators of inflammation

Because CARD14 signals together with ACT1 and TRAF6 to IL-17R-induced canonical NF-κB activation *(21)*, we next explored whether BCL10 and MALT1 are also involved in the IL-

17R proximal pathway. Surprisingly, although BCL10 and MALT1 were essential for IL-17A-induced cytokine production (Fig. 5B-I), both proteins were completely dispensable for IL-17A-induced IKK activation, for subsequent IκBα phosphorylation and for NF-κB p65 phosphorylation (**Fig. 6A-B**). In addition, we also observed normal IL-17A-induced p38 and JNK kinase activation in *Bcl10*- and *Malt1*-deficient keratinocytes (Fig. 6A-B). Likewise, although the BCL10/MALT1 complex controlled IL-1β and TNF-induced cytokine responses in keratinocytes (Fig. 5B-I), BCL10 was dispensable for IL-1β and TNF-induced IKK activation, IκBα phosphorylation and NF-κB p65 phosphorylation, as well as p38 and JNK activation (**Fig. 6C-D**). Thus, the BCL10/MALT1 signalosome is not involved in IL-17R-, IL-1R- or TNF receptor-induced proximal events that lead to canonical NF-κB, JNK or p38 activation.

To define the specific roles of BCL10 in keratinocyte responses, we next performed RNAseq analysis of *Bcl10*-proficient and *Bcl10*-deficient keratinocytes after IL-17A stimulation. First, we created an IL-17A response gene signature using a list of genes that are upregulated by IL-17A stimulation of normal human keratinocytes *(43)*, which we termed *IL17_NHEK*. As expected, IL-17A stimulation induced significant enrichment of this IL17_NHEK signature in both $Bcl10^{+/-}$ and $Bcl10^{-/-}$ murine keratinocytes, as shown by Gene Set Enrichment Analysis (GSEA) (**Fig. 6E** and **Fig. S5A**). However, direct comparison of $Bcl10^{+/-}$ and $Bcl10^{-/-}$ keratinocytes demonstrated a stronger enrichment of IL17_NHEK in *Bcl10* competent keratinocytes than in *Bcl10* deficient cells (**Fig. 6F** and **Fig. S5B**), demonstrating that BCL10 is required for full expression of the keratinocyte IL-17 response.

Because BCL10/MALT1 complexes can in principle amplify signals from inflammatory pathways by inactivating the negative inflammatory regulators A20 *(44)* and CYLD *(45)* in

multiple cell types, we next studied the proteolytic processing of these MALT1 substrates in primary murine keratinocytes. In line with published data *(46)*, we observed constitutive processing of both A20 and CYLD in wild-type keratinocytes, as demonstrated by faster-migrating specific bands in Western blots (**Fig. 6G-H**). Although A20 and CYLD processing was not further enhanced by IL-17A stimulation, it was absent in *Bcl10*- and *Malt1*-deficient keratinocytes (**Fig. 6G-H**), indicating that A20 and CYLD processing was indeed mediated by MALT1 protease activity. Consistent with this hypothesis, enforced activation of BCL10/MALT1 signaling in *Card11*$^{\Delta Linker\text{-}KC}$ keratinocytes enhanced A20 and CYLD cleavage (**Fig. 6I**). Furthermore, we also detected MALT1-mediated, constitutive proteolytic processing of the MALT1 substrate RelB *(47)* (**Fig. S5C**). Regnase-1 is an additional MALT1 substrate in lymphocytes *(48)*. Interestingly, IL-17A stimulation of *Bcl10*$^{-/-}$ and *Malt1*$^{-/-}$ keratinocytes induced normal degradation of Regnase-1 (**Fig. 6J-K**), which was previously demonstrated to be induced by IKK-mediated Regnase-1 phosphorylation *(49)*. Moreover, the absence of keratinocyte BCL10/MALT1 complexes allowed regular induction of the IL-17A target gene *Nfkbiz* (Fig. S4D-E), further indicating that the BCL10/MALT1 complex controls only selective keratinocyte responses to cytokines.

To directly evaluate whether the failure to inactivate negative regulators of inflammation underlies the decreased cytokine production in *Bcl10*- or *Malt1*-deficient keratinocytes, we next inactivated the stabilized A20 in *Bcl10*$^{-/-}$ keratinocytes using RNA interference (**Fig. 7A**). Indeed, siRNA-mediated A20 inactivation allowed normal IL-17A-induced *Cxcl5* and *Csf2* expression in *Bcl10*-deficient keratinocytes and increased the expression of *Tnf* (**Fig. 7B-D**). This effect was however not due to altered expression of *Il17ra* and *Traf3ip2* (encoding for ACT1), since their expression was not altered by the presence of BCL10 or A20 (**Fig. S6A-B**). Furthermore, not all

IL-17A responses were affected, as BCL10-independent induction of *Nfkbiz* was not increased upon A20 siRNA treatment (**Fig. 7E**).

Next, we utilized keratinocytes from an additional knock-in mouse line that harbors a point mutation in the MALT1 catalytic domain (*Malt1 paracaspase-mutant* or $Malt1^{PM}$ mice), in which the MALT1 protein is expressed from the endogenous *Malt1* locus at normal levels and is able to assemble into BCL10/MALT1 complexes but is specifically impaired in its proteolytic functioning *(50)*. Keratinocytes from $Malt1^{PM/-}$ mice showed severely diminished upregulation of *Tnf*, *Cxcl5* and *Csf2* upon IL-17A stimulation (**Fig. 7F-H**), demonstrating on a genetic level that the proteolytic function of MALT1 is key for the keratinocyte inflammatory response.

To explore the role of the MALT1 protease in the increased cytokine responses in keratinocytes with activated BCL10/MALT1 signaling, we then pharmacologically inhibited the MALT1 proteolytic function in $Card11^{\Delta Linker\text{-}KC}$ keratinocytes with mepazine *(51, 52)*. Mepazine treatment led to diminished IL-17A-induced *Tnf*, *Cxcl5* and *Csf2* expression but did not interfere with the upregulation of *Nfkbiz* (**Fig. S6C-F**). A comparable effect was observed in mepazine-treated $Card14^{\Delta E138}$ keratinocytes (**Fig. S6G-J**). Finally, to study the keratinocyte-intrinsic functions of the MALT1 protease in skin inflammation *in vivo*, we engineered mice that expressed protease-mutated MALT1 together with $CARD11^{\Delta Linker}$ only in keratinocytes but not in other cell types ($Card11^{\Delta Linker\text{-}KC};Malt1^{PM\text{-}KC}$ mice). Keratinocyte-intrinsic MALT1 protease inactivation strongly attenuated psoriasiform skin inflammation, as $Card11^{\Delta Linker\text{-}KC};Malt1^{PM\text{-}KC}$ mice exhibited significantly reduced ear swelling (**Fig. 7I**), local inflammatory cytokine production (**Fig. 7J**) and neutrophil infiltration (**Fig. 7K**).

Keratinocyte BCL10/MALT1 signalosomes are active in sporadic psoriasis

Overall, our analysis in clean genetic mouse models established essential keratinocyte-intrinsic functions of BCL10/MALT1 signaling in inflammatory responses beyond putative selective effects of inherited *CARD14-GOF* alterations in the IL-17R proximal pathway. Since these BCL10/MALT1-mediated functions are required for the amplification of multiple inflammatory signals and sufficient to drive psoriasiform skin inflammation, we speculated that keratinocyte BCL10/MALT1 signaling could also play a broader role in human sporadic psoriasis. To explore this hypothesis in primary human psoriasis skin specimens, we first established a transcriptomic signature of BCL10/MALT1 activation (**Fig. 8A**). To this end, we performed RNA sequencing in murine keratinocytes with genetically enforced (CARD11$^{\Delta Linker}$-driven) BCL10/MALT1 activity and in wild-type keratinocytes. We termed the set of 293 significantly upregulated genes (log2-fold change > 1.5 and FDR < 0.05) that were induced by BCL10/MALT1 activity *BM_activation_KC_UP* (Fig. 8A). Using this signature for single sample GSEA on ca. 800 human cell lines (**Fig. S7A-C**), we found that although *Bcl10* itself was not part of the 293 genes defining *BM_activation_KC_UP*, *BCL10* expression positively correlated with *BM_activation_KC_UP* in this large data set. Therefore, we first analyzed *BCL10* mRNA expression in three independent transcriptomic data sets from human psoriatic lesional skin and healthy donor skin (**Fig. 8B**). Interestingly, we detected significantly higher *BCL10* expression in psoriatic skin than in healthy skin in all three data sets (**Fig. 8C**). Moreover, upon comparing transcriptomes from paired lesional and nonlesional skin samples of sporadic psoriasis patients in three additional data sets (**Fig. 8D**), *BCL10* gene expression was significantly higher in the lesional than in the nonlesional skin (**Fig. 8E**). Next, we studied BCL10 protein expression in a series of skin samples from sporadic psoriasis patients using immunohistochemistry. Interestingly, BCL10

protein expression was significantly increased in lesional epidermal keratinocytes compared with paired nonlesional epidermal keratinocytes (**Fig. 8F-G**). Moreover, we also found significantly increased *MALT1* expression in psoriatic skin compared to healthy control skin (**Fig. S8A**), as well as in psoriatic lesional skin compared to the paired non-lesional skin of sporadic psoriasis patients (**Fig. S8B**). Encouraged by these results, we next performed GSEA with the *BM_activation_KC_UP* gene signature in human sporadic psoriasis. A significant positive enrichment of *BM_activation_KC_UP* was observed in psoriatic lesional skin in comparison to healthy donor skin in the investigated datasets (**Fig. 8H**).

Functional annotation of the 293 target genes of enforced BCL10/MALT1 signaling in keratinocytes (Fig. 8A) revealed a significant positive enrichment (FDR < 0.1) of nine KEGG pathways (Kyoto Encyclopedia of Genes and Genomes), which included TNF, Toll-like receptor and chemokine signaling pathways, as well as molecular pathways induced by various viruses (**Table S1**). Interestingly, eight out of these nine BCL10/MALT1-triggered KEGG signatures were previously established as bona fide characteristics of human psoriatic skin lesions *(53)* (**Fig. 8I**). Conversely, GSEA with the significantly enriched KEGG pathways in human lesional psoriatic skin *(53)* revealed that 10 out of the 12 pathways with murine counterparts were also enriched upon enforced BCL10/MALT1 signaling in murine CARD11$^{\Delta Linker}$-expressing keratinocytes (**Fig. 8K**). Together, these results provide the first indications of aberrant BCL10/MALT1 signaling in lesional keratinocytes from sporadic human psoriasis patients.

DISCUSSION

Activating *CARD14* mutations are found in rare cases of familial psoriasis and pityriasis rubra pilaris patients *(7, 9–11)*, and respective mutations in the mouse germline *(19–21)* or in keratinocytes *(22)* are sufficient to drive psoriasiform skin inflammation *in vivo* with characteristics of the human disease psoriasis. By conditionally deleting *Bcl10* or *Malt1* only in keratinocytes in germline mutant mice that harbor pathogenic *Card14*$^{\Delta E138}$ mutation in all cell types, we unequivocally demonstrate that the keratinocyte-intrinsic function of the BCL10/MALT1 complex is absolutely essential to drive CARD14-GOF-induced skin inflammation. Thus, aberrant signaling in other putatively CARD14-expressing cell types, such as Langerhans cells, dermal γδ T cells or dermal endothelial cells, is largely negligible for the pathogenesis of this severe inherited disorder.

Since CARD14 can signal together with TRAF6 and ACT1 in the IL-17R proximal pathway *(21)*, disease-associated CARD14 variants have been considered a pathophysiological link between psoriatic IL-17A stimulation and inflammatory IKK-mediated NF-κB activation *(17, 21, 23)*. We now provide the first molecular evidence that BCL10 and MALT1, in contrast to CARD14 *(21)*, are not involved in the IL-17R proximal TRAF6/ACT1 cascade, since IL-17A stimulation of primary *Bcl10*- or *Malt1*-deficient keratinocytes triggers regular IKK activation and normal IκBα phosphorylation and degradation. Likewise, IL-17A-induced MAPK signaling, which is defective in *Card14*$^{-/-}$ keratinocytes *(21)*, is also intact in *Bcl10*$^{-/-}$ or *Malt1*$^{-/-}$ keratinocytes. In contrast, our study reveals a much more pleiotropic role for BCL10/MALT1 complexes in keratinocyte inflammatory signaling, as these complexes strongly amplify pathophysiological outputs from a series of psoriasis-relevant cytokines, including IL-17A but also

IL-1β and TNF, and potentially others by releasing A20 and CYLD inhibition, presumably in the proximity of cytokine-activated inflammatory signalosomes. Consistent with this model, the blunted inflammatory responses in *Bcl10*-deficient keratinocytes could be restored by inactivating A20. Of note, A20 and CYLD have previously been established as bona fide MALT1 proteolytic targets *(44, 45)*, and A20 and its interacting protein TNIP1 (also known as ABIN1) *(3)* as well as CYLD are also located within genetic loci associated with psoriasis susceptibility *(54)*. Moreover, epidermal loss of A20 or TNIP1 facilitates psoriasiform inflammation in mice *(55, 56)* even in the absence of *CARD14* mutations.

In addition to demonstrating an intrinsic requirement of BCL10/MALT1 signaling and protease activity for keratinocyte inflammatory responses, we also provide conclusive genetic evidence that the selective keratinocyte-intrinsic enforcement of BCL10/MALT1 activity with an artificial CARD11$^{\Delta Linker}$ engager molecule is sufficient to drive psoriasiform skin inflammation that features the key characteristics of the human disease on a histopathological, cellular and molecular signature level. Thus, BCL10/MALT1 signalosomes themselves can in principle function at the origin of the psoriatic inflammatory cascade. Based on our genetic findings in conditional knock-in and knockout mice in the presence or absence of lymphocytes (*Rag2*$^{-/-}$), we propose two distinct functions for BCL10/MALT1 signalosomes within keratinocytes in psoriasis (summarized in **Fig. 8K**). First, pathological activation of BCL10/MALT1 signaling within keratinocytes can provoke acanthosis and hyperkeratosis and trigger inflammatory responses with cell-autonomous NF-κB activation and high levels of inflammatory cytokine production. Subsequently, these events can promote a Th17-dominated lymphocytic reaction. While acanthosis and hyperkeratosis are also detected in the absence of inflammatory leukocytes, the presence and recruitment of lymphocytes and the production of IL-17A – presumably by

infiltrating αβ T cells – are required to drive psoriasiform skin inflammation and maintain the full phenotype, as the pathology does not develop in a *Rag2*-deficient background and is strongly ameliorated by treatment with anti-IL-17A. These data are further corroborated by the findings that the psoriasiform phenotype of different *Card14-GOF* mouse models is also reversed upon IL-23 or IL-17A blockade *(19, 21)*. Moreover, in the presence of lymphocyte-mediated inflammatory conditions, the keratinocyte-intrinsic BCL10/MALT1 complex has a second key function, as it inactivates inhibitory factors such as A20 and CYLD through MALT1 protease activity. Therefore, the BCL10/MALT1 signalosome licenses pathogenic keratinocytes to fully respond to multiple exogenous inflammatory stimuli, such as IL-17A, IL-1β or TNF, with potent production of additional cytokines and chemokines that subsequently attract and stimulate neutrophils to propel a vicious cycle to exaggerate debilitating skin disorders.

Based on this model, we speculated that BCL10/MALT1 signaling could have a broader role in psoriasis beyond rare familial *CARD14-GOF*-associated cases *(57)*. This hypothesis is indeed supported by enhanced *BCL10* and *MALT1* gene expression in lesional compared with nonlesional skin from sporadic psoriasis patients, which positively correlates with BCL10/MALT1 activity in a large series of human cell lines. Based on *in silico* prediction the promoter region of *BCL10* contains binding sites for the NF-κB transcription factor p65 *(58)*, which is highly active in the lesional psoriatic skin *(59)*. Therefore, we speculate that the increase in *BCL10* in the lesional psoriatic skin might be mediated via NF-κB / p65 activity, potentially in a positive feedback loop. In addition, and more significantly, transcriptomic profiling of human psoriatic lesional skin also revealed an intriguing enrichment of the pathogenic BCL10/MALT1 triggered gene expression signature, which is characterized by the specific activation of most of the established hallmark KEGG signatures of psoriasis *(53)*. Together, these data suggest that uncharacterized

environmental and host factors might pathologically activate keratinocyte-intrinsic BCL10/MALT1 complexes in psoriasis to promote pathological crosstalk between a damaged or stressed epidermis and the immune system during the initiation and/or amplification of skin inflammation. Since keratinocytes can respond to fungal cell wall components or pathogen-associated molecular patterns from *Staphylococcus aureus* with the activation of BCL10/MALT1 signaling in response to innate immune receptor triggering *(26)* and furthermore express, in addition to CARD14, its homologue CARD10 *(46),* which can induce BCL0/MALT1 activity upon the stimulation of G-protein-coupled or growth factor receptors *(46)*, it is conceivable that such BCL10/MALT1 activators could be of either microbial or sterile origin. While these factors need to be defined in future studies, the bacterial and fungal microbiomes could play an instigating function in the stimulation of these pathways, as there is considerable evidence that alterations in the skin microbiome could play a decisive role in the pathogenesis of psoriasis *(60)* and that the yeast *Malassezia furfur* is more abundant in psoriatic skin than in healthy skin *(61, 62)*. In addition to rare CARD14-GOF variants, common variants have also been associated with sporadic psoriasis *(57)*. Nevertheless, *in vitro* studies of common variants have so far failed to demonstrate increased activity *(57)*. Therefore, whether these variants contribute to the observed activation of BCL10/MALT1 complexes in lesional psoriatic skin needs to be further investigated.

In conclusion, rare, monogenic diseases have frequently provided key insights into biological pathways that enhance our understanding of common complex traits. While activating *CARD14-GOF* mutations are found in individual cases of familial inflammatory skin diseases, they not only signal via TRAF6/ACT1 in the IL-17R pathway but also interact with BCL10 and MALT1 and trigger the activation of BCL10/MALT1 signaling with NF-κB and paracaspase activation *(18, 22, 25, 26)*. By mechanistically demonstrating in clean genetic models that

BCL10/MALT1 complexes play a more general role in inflammatory keratinocyte signaling, our data provide a rationale to further explore the mechanisms and consequences of keratinocyte BCL10/MALT1 signaling in sporadic psoriasis. Since MALT1 protease activity is critical for inflammatory keratinocyte responses and MALT1 protease inhibitors are in preclinical and clinical development for lymphoma treatment (ClinicalTrials.gov Identifier: NCT03900598), our study also recommends to explore the utility of such inhibitors for the treatment of sporadic psoriasis.

MATERIALS AND METHODS

Study design

This was a preclinical and translational study on the role of keratinocyte BCL10/MALT1 complexes in psoriasiform skin inflammation. Genetically engineered mice were crossed and the resulting skin phenotype was characterized by measurement of ear thickness and gene expression, histopathological examination and flow cytometric evaluation of infiltrating immune cells. Mice of both sexes, newborn or aged 8-16 weeks, were used for all experiments. Littermate controls were used whenever possible. For *in vitro* experiments, keratinocytes were isolated from newborn mice, cultured and stimulated with cytokines, followed by gene expression analysis and cytokine beads assays. *Rosa26*$^{LSL\text{-}Card11\Delta Linker}$ mice contain the cDNA of a constitutive active variant of the murine *Card11* gene (the linker domain was excised) in the ubiquitously expressed *Rosa26* gene locus. For the transcriptional analysis of human skin samples, publicly available datasets of the skin samples of psoriasis patients and healthy donors from the Gene Expression Omnibus were used. For the immune histology, skin samples of psoriasis patients treated at the Department of Dermatology at the Technical University of Munich were analyzed.

Mice

For the generation of *Rosa26*$^{LSL\text{-}Card11\Delta Linker}$ mice, the cDNA of the murine *Card11* gene without the linker domain *(32)* was cloned into a Rosa26-targeting vector *(63)*, in which it was preceded by loxP-STOP-loxP sequences to allow for conditional expression (Fig. S2A), and followed by the cDNA sequence of enhanced GFP. The targeting vector was linearized and electroporated into E14K murine embryonic stem cells, followed by clone selection. The clones were analyzed for homologous recombination by Southern blotting using a 5'-flanking Rosa26

probe of the following sequence: 5' gat caa aac act aat gaa ctt taa gtc ctg tga agg gta aaa cct cag ata gta aca aaa agc ttc caa ccc ctc ctc aaa caa aaa acc cca agt ctt taa ctt tga tcc agt ttt cag atg ctg ata tcc ata aat gga tac agt tat gaa ttg cta att ctg gtc tct tca cta gca aaa agc aaa gca gct cag cag tac aat ttc cca gga aag caa gca agg ttt ctt tcc agc ctg agc agc cat cac taa gtg cag ttc cct gca gcc aac agc att aat gga cgc tgc act gct gtc ctt ccc tgg aga cag cag cca gca cta ctc aag ctt ctc acg tag caa cca gag ctc cag agc cag cag ctg ctg ccg cct tgt ata ctc act cct gtg atc caa cac agg agc aac ctt ttc ttt acc cca ccc cca ctt ctt aac aca ctt ttt ttt ggg ggg ggg ggg gaa caa gtg ctc cat gct gga agg att gga act atg ctt tta gaa agg aac aat cct aag gtc act ttt aaa ttg agg tct ttg att tga aaa tca aca aat acc aaa ttc caa ata ttc gtt tta att aa 3' (Fig. S2B) *(64)*. The blastocyst injection of the clones (performed by PolyGene) and subsequent chimera breeding resulted in *Rosa26*$^{LSL\text{-}Card11\Delta Linker}$ mice.

Bcl10$^{-/-}$, *Malt1*$^{-/-}$, *Bcl10*^{floxed}, *Malt1*^{floxed} and *Malt1*^{PM} mice have been previously described *(27, 39, 40, 50)*. To conditionally ablate and/or express genes in epithelial cells, *K14Cre* mice *(28)* were used, which were purchased from the Jackson Laboratory [Tg (KRT14-cre) 1Amc/J]. *Rag2*$^{-/-}$ and *Card14*$^{\Delta E138}$ mice were also obtained from the Jackson Laboratory [B6(Cg)-Rag2$^{tm1.1Cgn/J}$ and C57BL/6J-Card14^{em9Lutzy}/J] *(19, 35)*.

Experimentally induced psoriasis-like dermatitis and neutralization of IL-17A

Aldara^{TM} (5% Imiquimod) cream (50 mg and 5 mg) was applied to Nair^{TM} crème-treated dorsal skin and ears of 8- to 9-week-old mice daily for 5 days, respectively. Control mice were treated with Nair^{TM} and Vaseline crème. The ear and dorsal skin thicknesses were measured using a digital micrometer. The mice were sacrificed on day 6. For the antibody-blocking experiments, 200 μg of anti–IL-17A (Novartis) or 200 μg of anti-Ciclosporin A control antibody was injected

intraperitoneally into 12-week-old mice every other day for two weeks. Mice were randomized in all *in vivo* experiments. The mice were sacrificed on day 14.

Analysis with flow cytometry

For single-cell suspensions derived from skin, the dorsal and ventral parts of the ears were separated. The ear skin halves and dorsal skin were then processed as previously described *(65)*. They were briefly digested with dispase II (Sigma-Aldrich) then with collagenase and DNAse I (both from Roche) and filtered through a 70-µm nylon mesh. Cell suspensions were separated using Percoll density gradient centrifugation. For intracellular cytokine staining, cells were stimulated with phorbol 12-myristate 13-acetate (80 ng/mL) and ionomycin (1 µM, both from Sigma-Aldrich). One hour later, they were treated with brefeldin A (eBioscience) and incubated for 4 hours at 37 °C. For the IL-17R staining *in vitro* cultured keratinocytes were detached using Trypsin-EDTA 0,05% (Gibco). The cells were stained with a fixable viability dye (eBioscience) and the following antibodies for flow cytometric analysis: CD3ε (145-2C11, #25-0031-82), CD4 (GK1.5, #11-0041-82), CD8a (53-6.7, #45-0081-82), CD11b (M1/70, #48-0112-82), CD45 (30-F11, #48-0451-82 and #45-0451-82), CD217/IL-17Ra (PAJ-17R, #17-7182-82), IL-17A (eBio17B7, #12-7177-81), Ly6G (1A8, #12-9668-82), TCRβ (H57-597, #47-5961-82) and TCRγδ (GL3, #17-5711-82, all from eBioscience). The data were collected with a FACSCanto II cytometer (BD Biosciences) and analyzed using FlowJo software (Tree Star).

Histology

Mouse ear biopsy specimens were fixed with 10% phosphate-buffered formalin, embedded in paraffin and stained with H&E according to standard procedures. Immunohistochemistry of human skin biopsy specimens was performed with anti-BCL10 (331.3,

Santa Cruz) antibody using a Bond RXm (Leica, Wetzlar, Germany) system with a Polymer Refine Detection system. The psoriasis scores were evaluated according to Baker et al. *(33)*.

Quantitative reverse transcription PCR

RNA was isolated from the ear and dorsal skin of mice using TRIzol (Invitrogen) and from cultured cells using RLT Buffer from an RNeasy kit (Qiagen). cDNA was generated using a QScript cDNA synthesis kit (QuantaBio), and quantitative real-time PCR was performed using Takyon No ROX SYBR 2X MasterMix (Eurogentec) on a LightCycler Instrument II (Roche). All murine and human PCR data were normalized to the *Gapdh* and *RPLP0* values, respectively. Primer sequences used are the followings (5' – 3'): Murine: *Gapdh*: gtg ttc cta ccc cca atg tg , ggt cct cag tgt agc cca ag; *Il17a:* atc cct caa agc tca gcg tgt c, ggg tct tca ttg cgg tgg aga g; *Il4:* ggt ctc aac ccc cag cta gt, gcc gat gat gat ctc tct caa gtg at; *Ifng:* gcc acg gca cag tca ttg a, tgc tga tgg cct gat tgt ctt; *Ccl20:* gcc tct cgt aca tac aga cgc, cca gtt ctg ctt tgg atc agc; *Csf2:* ggc ctt gga agc atg tag agg, gga gaa ctc gtt aga gac gac tt; *Cxcl1:* ccc act gca ccc aaa ccg aag, cag gtg cca tca gag cag tct gt; *Cxcl5:* gct gcc cct tcc tca gtc at, cac cgt agg gca ctg tgg ac; *Lcn2:* aca ttt gtt cca agc tcc agg gc, cat ggc gaa ctg gtt gta gtc cg; *S100a8:* aaa tca cca tgc cct cta caa g, ccc act ttt atc acc atc gca a; *Tnf:* atg agc aca gaa agc atg atc, tac agg ctt gtc act cga att; *Nfkbiz:* tgc tac aca tcc gaa gca aca, cac tgc act ctt cag gtc tgt; *Krt6a:* aga gag ggg tcg cat gaa ct, tca tct gtt aga ctg tct gcc tt; *Krt6b:* agt gcc ctg tgt acg ggg tcg tg, aca gag gta ggg agg gag gag cct; *Krt16* gag atc aaa gac tac agc cc, cat tct cgt act tgg tcc tg. Human: *RPLP0:* tcg aca atg gca gca tct ac, gcc ttg atg gca gca ag; *CXCL5:* tgg acg acc ttt tca agg; ctt ccc tgg gtt cag aga c; *CSF2:* tcc tga acc tga gta gag aca c, tgc tgc ttg tag tgg ctg g; *TNF:* tct tct cga acc ccg agt ga, cct ctg atg gca cga cca g, *CARD14:* cgg gca ctt gct gga ttt g, tcc atg aga ccg cta aag tta ct.

Immunoblotting

Cells were lysed for immunoblotting in RIPA buffer containing protease & phosphatase inhibitors (Calbiochem) at the indicated time points. For the detection of a RelB cleavage product, cells were pretreated with 20μM MG132 (Sigma-Aldrich) for 60 minutes. The following antibodies were used: pIKK1/2 (16A6), pIκBα (5A5), pp65 (93H1), pp38 (D3F9), pJNK (81E11), BCL10 (C78F1), A20 (D13H3), RelB (C1E4), tubulin (11H10, all from Cell Signaling Technologies), CYLD (E-10, Santa Cruz), and Regnase-1 (MAB7875, R&D).

Isolation and culture of keratinocytes

Murine keratinocytes were isolated from neonatal mice as described in Li et al. *(66)* and cultured in calcium-free keratinocyte SFM (Gibco) supplemented with 0.05 mM $CaCl_2$ in collagen-coated (collagen IV from human placenta, Sigma-Aldrich) flasks. Human keratinocytes were obtained from the skin of healthy individuals. The epidermis was separated from the dermis following overnight digestion with dispase (Roche Diagnostics) and then incubated in 0.05% trypsin to obtain keratinocytes, which were cultured in EpiLife Medium (60 μM $CaCl_2$) supplemented with Defined Growth Supplement (both from Thermo Fischer).

Stimulation, RNA interference and MALT1 protease inhibition in keratinocytes

Recombinant murine IL-17A (200 ng/mL), TNF (100 ng/mL) IL-1β (10 ng/mL) and human IL-17A (50 ng/μL, all from PeproTech) were used for the stimulation experiments. For RNA interference, keratinocytes were transfected with MISSION® esiRNA against A20, BCL10 or GFP (Sigma-Aldrich) or with Silencer® Select siRNA against CARD14 or GAPDH (Thermo Fisher) using Lipofectamine 3000 (Thermo Fisher) 72 hours in advance of stimulation. To inhibit

MALT1 paracaspase activity, cells were treated with 10 μM/mL mepazine (Sigma-Aldrich) for 6 hours before stimulation. The cells were harvested for RT-PCR analysis, and the supernatants were used for cytokine bead assays 5 hours after cytokine stimulation.

Cytokine bead assay

TNF levels in cell culture supernatants were determined using a Mouse TNF Enhanced Sensitivity Flex Set Kit (BD Biosciences) according to the manufacturer's instructions. The data were collected with a FACSCanto II cytometer (BD Biosciences) and analyzed with FlowJo software (Tree Star).

NF-κB luciferase reporter assay

Keratinocytes were transfected with NF-κB luciferase reporter and PRL-TK (Promega) plasmids using Lipofectamine 3000 (Thermo Fisher Scientific). Luciferase activity was measured using the Dual-Glo Luciferase Assay System (Promega).

Transcriptome analyses

For the RNAseq analyses, keratinocytes were isolated, cultured and stimulated, and total RNA was isolated as described above. Library preparation from 100 ng of total RNA was performed using the NEBNext® Ultra™ II RNA Library Prep Kit for Illumina® and NEBNext® Poly(A) mRNA Magnetic Isolation Module (New England Biolabs), and SE-75 bp sequencing was performed on an Illumina NextSeq550 machine using NextSeq 500/550 High Output Kit v2.5 cartridges (Illumina, San Diego, California, USA). Reads were aligned to the mm10 genome using HISAT2 *(67)*, and transcriptome assembly was performed using StringTie *(68)*. Differential expression was assessed with Deseq2 *(69)*, and the list of differentially expressed genes was

defined as log2-fold change > 1.5 and FDR < 0.05. Functional annotation of differentially expressed genes was performed using DAVID software (https://david.ncifcrf.gov/) *(70, 71)*. GSEA was performed with GSEA software *(72, 73)*. The following data sets from the Gene Expression Omnibus were analyzed: GSE114286 (9 healthy controls and 18 psoriatic skin samples), GSE54456 (82 healthy controls and 92 psoriatic skin samples), GSE66511 (12 healthy controls and 12 paired psoriatic lesional and nonlesional skin samples) and GSE53552 (24 paired psoriatic lesional and nonlesional skin samples).

Correlation analysis of *BCL10* expression and CBM activation

To investigate whether *BCL10* expression correlates with the activation of BCL10/MALT1 complexes, we turned to the Cancer Cell Line Encyclopedia (CCLE) database, which contains transcriptomic data of 1077 human cell lines, and performed single sample GSEA to look for enrichment of the BM_activation_KC_UP gene set in each cell line. Pearson's linear regression analysis was used to examine a correlation between enrichment of the BM_activation_KC_UP signature and *Bcl10* expression. The analyzed cell lines are highly heterogeneous; therefore, the observed correlation may theoretically derive from inherent differences in *Bcl10* expression among the different cell line types. Thus, we stratified the cell lines based on their "origin" using their tgca code and reran the abovementioned analyses (Fig. S7). We included gene sets of the Molecular Signatures Database containing genes upregulated upon NF-κB activation (a direct consequence of BCL10/MALT1 activation), and we also generated a sub-list of the BM_activation_KC_UP gene set by filtering for genes involved in immune functions (Fig. S7C). In most, albeit not in all cell line groups, *Bcl10* expression significantly and positively correlated with the enrichment scores of both NF-κB activation and the BCL10/MALT1 activation signatures (Fig. S7C).

Statistical Analysis

Statistical tests were performed using GraphPad PRISM. The statistical tests are described in the respective figure legends. Error bars represent standard deviation. P values <0.05 were considered statistically significant.

Study approval

Human keratinocytes were isolated from clinically healthy skin samples from patients undergoing elective operations, while immunohistochemical staining was performed on skin samples collected from psoriasis patients. Samples were collected at the Department of Dermatology and Allergy, Technical University of Munich upon informed consent. Ethics approval was obtained from the Institutional Review Board of the Technical University of Munich (reference number 82/19S). All work was carried out in accordance with the Declaration of Helsinki for experiments involving humans. All animal work was conducted in accordance with the German Federal Animal Protection Laws and approved by the government of Upper Bavaria (Regierung von Oberbayern, Munich, Germany, ROB-55.2-2532.Vet_02-15-26 and ROB-55.2-2532.Vet_02-19-24).

SUPPLEMENTARY MATERIALS

Fig. S1. Keratinocyte-intrinsic BCL10/MALT1 signaling mediates mutant CARD14-triggered skin inflammation

Fig. S2. Generation of a mouse with conditional CARD11$^{\Delta Linker}$ expression

Fig. S3. BCL10/MALT1 activation in keratinocytes drives psoriasiform skin inflammation

Fig. S4. BCL10/MALT1 signaling in keratinocytes amplifies secondary cytokine circuits

Fig. S5. BCL10/MALT1 signalosomes in keratinocytes inhibit specific negative regulators of inflammation

Fig. S6. MALT1 paracaspase facilitates keratinocyte inflammatory responses by cleaving negative regulators and thus controls the magnitude of keratinocyte cytokine responses

Fig. S7. *BCL10* expression correlates with the transcriptomic changes induced by activation of BCL10/MALT1 signalosomes

Fig. S8. *MALT1* expression is increased in the lesional psoriatic skin

Table S1. Enriched KEGG pathways in *Card11*$^{\Delta Linker\text{-}KC}$ keratinocytes using DAVID analysis (FDR < 25%)

Supplementary Methods

REFERENCES AND NOTES

1. C. E. Griffiths, J. N. Barker, Pathogenesis and clinical features of psoriasis, *The Lancet* **370**, 263–271 (2007).

2. J. Takeshita, S. Grewal, S. M. Langan, N. N. Mehta, A. Ogdie, A. S. Van Voorhees, J. M. Gelfand, Psoriasis and Comorbid Diseases Part I. Epidemiology, *J. Am. Acad. Dermatol.* **76**, 377–390 (2017).

3. R. P. Nair, K. C. Duffin, C. Helms, J. Ding, P. E. Stuart, D. Goldgar, J. E. Gudjonsson, Y. Li, T. Tejasvi, B. J. Feng, A. Ruether, S. Schreiber, M. Weichenthal, D. Gladman, P. Rahman, S. J. Schrodi, S. Prahalad, S. L. Guthery, J. Fischer, W. Liao, P.-Y. Kwok, A. Menter, G. M. Lathrop, C. A. Wise, A. B. Begovich, J. J. Voorhees, J. T. Elder, G. G. Krueger, A. M. Bowcock, G. R. Abecasis, Genomewide Scan Reveals Association of Psoriasis with IL-23 and NF-κB Pathways, *Nat. Genet.* **41**, 199–204 (2009).

4. L. C. Tsoi, S. L. Spain, J. Knight, E. Ellinghaus, P. E. Stuart, F. Capon, J. Ding, Y. Li, T. Tejasvi, J. E. Gudjonsson, H. M. Kang, M. H. Allen, R. McManus, G. Novelli, L. Samuelsson, J. Schalkwijk, M. Ståhle, A. D. Burden, C. H. Smith, M. J. Cork, X. Estivill, A. M. Bowcock, G. G. Krueger, W. Weger, J. Worthington, R. Tazi-Ahnini, F. O. Nestle, A. Hayday, P. Hoffmann, J. Winkelmann, C. Wijmenga, C. Langford, S. Edkins, R. Andrews, H. Blackburn, A. Strange, G. Band, R. D. Pearson, D. Vukcevic, C. C. Spencer, P. Deloukas, U. Mrowietz, S. Schreiber, S. Weidinger, S. Koks, K. Kingo, T. Esko, A. Metspalu, H. W. Lim, J. J. Voorhees, M. Weichenthal, H. E. Wichmann, V. Chandran, C. F. Rosen, P. Rahman, D. D. Gladman, C. E. Griffiths, A. Reis, J. Kere, R. P. Nair, A. Franke, J. N. Barker, G. R. Abecasis, J. T. Elder, R. C. Trembath, Identification of fifteen new psoriasis susceptibility loci highlights the role of innate immunity, *Nat. Genet.* **44**, 1341–1348 (2012).

5. S. K. Mahil, F. Capon, J. N. Barker, Genetics of Psoriasis, *Dermatol. Clin.* **33**, 1–11 (2015).

6. N. Dand, S. Mucha, L. C. Tsoi, S. K. Mahil, P. E. Stuart, A. Arnold, H. Baurecht, A. D. Burden, K. Callis Duffin, V. Chandran, C. J. Curtis, S. Das, D. Ellinghaus, E. Ellinghaus, C. Enerback, T. Esko, D. D. Gladman, C. E. M. Griffiths, J. E. Gudjonsson, P. Hoffman, G. Homuth, U. Hüffmeier, G. G. Krueger, M. Laudes, S. H. Lee, W. Lieb, H. W. Lim, S. Löhr, U. Mrowietz, M. Müller-Nurayid, M. Nöthen, A. Peters, P. Rahman, A. Reis, N. J. Reynolds, E. Rodriguez, C. O. Schmidt, S. L. Spain, K. Strauch, T. Tejasvi, J. J. Voorhees, R. B. Warren, M. Weichenthal, S. Weidinger, M. Zawistowski, R. P. Nair, F. Capon, C. H. Smith, R. C. Trembath, G. R. Abecasis, J. T. Elder, A. Franke, M. A. Simpson, J. N. Barker, Exome-wide association study reveals novel psoriasis susceptibility locus at TNFSF15 and rare protective alleles in genes contributing to type I IFN signalling, *Hum. Mol. Genet.* **26**, 4301–4313 (2017).

7. C. T. Jordan, L. Cao, E. D. O. Roberson, K. C. Pierson, C.-F. Yang, C. E. Joyce, C. Ryan, S. Duan, C. A. Helms, Y. Liu, Y. Chen, A. A. McBride, W.-L. Hwu, J.-Y. Wu, Y.-T. Chen, A. Menter, R. Goldbach-Mansky, M. A. Lowes, A. M. Bowcock, PSORS2 Is Due to Mutations in CARD14, *Am. J. Hum. Genet.* **90**, 784–795 (2012).

8. C. T. Jordan, L. Cao, E. D. O. Roberson, S. Duan, C. A. Helms, R. P. Nair, K. C. Duffin, P. E. Stuart, D. Goldgar, G. Hayashi, E. H. Olfson, B.-J. Feng, C. R. Pullinger, J. P. Kane, C. A. Wise, R. Goldbach-Mansky, M. A. Lowes, L. Peddle, V. Chandran, W. Liao, P. Rahman, G. G. Krueger, D. Gladman, J. T. Elder, A. Menter, A. M. Bowcock, Rare and Common Variants in CARD14, Encoding an Epidermal Regulator of NF-kappaB, in Psoriasis, *Am. J. Hum. Genet.* **90**, 796–808 (2012).

9. M. Ammar, C. Bouchlaka-Souissi, C. a. Helms, I. Zaraa, C. t. Jordan, H. Anbunathan, R. Bouhaha, S. Kouidhi, N. Doss, R. Dhaoui, A. Ben Osman, A. Ben Ammar El Gaied, R. Marrakchi, M. Mokni, A. m. Bowcock, Genome-wide linkage scan for psoriasis susceptibility loci in multiplex Tunisian families, *Br. J. Dermatol.* **168**, 583–587 (2013).

10. M. Ammar, C. t. Jordan, L. Cao, E. Lim, C. Bouchlaka Souissi, A. Jrad, I. Omrane, S. Kouidhi, I. Zaraa, H. Anbunathan, M. Mokni, N. Doss, E. Guttman-Yassky, A. B. El Gaaied, A. Menter, A. m. Bowcock, CARD14 alterations in Tunisian patients with psoriasis and further characterization in European cohorts, *Br. J. Dermatol.* **174**, 330–337 (2016).

672 11. D. Fuchs-Telem, O. Sarig, M. A. M. van Steensel, O. Isakov, S. Israeli, J. Nousbeck, K. Richard, V.
673 Winnepenninckx, M. Vernooij, N. Shomron, J. Uitto, P. Fleckman, G. Richard, E. Sprecher, Familial Pityriasis
674 Rubra Pilaris Is Caused by Mutations in CARD14, *Am. J. Hum. Genet.* **91**, 163–170 (2012).

675 12. Q. Li, H. J. Chung, N. Ross, M. Keller, J. Andrews, J. Kingman, O. Sarig, D. Fuchs-Telem, E. Sprecher, J. Uitto,
676 Analysis of CARD14 Polymorphisms in Pityriasis Rubra Pilaris: Activation of NF-κB, *J. Invest. Dermatol.* **135**,
677 1905–1908 (2015).

678 13. T. Takeichi, K. Sugiura, T. Nomura, T. Sakamoto, Y. Ogawa, N. Oiso, Y. Futei, A. Fujisaki, A. Koizumi, Y.
679 Aoyama, K. Nakajima, Y. Hatano, K. Hayashi, A. Ishida-Yamamoto, S. Fujiwara, S. Sano, K. Iwatsuki, A. Kawada,
680 Y. Suga, H. Shimizu, J. A. McGrath, M. Akiyama, Pityriasis Rubra Pilaris Type V as an Autoinflammatory Disease
681 by CARD14 Mutations, *JAMA Dermatol.* (2016), doi:10.1001/jamadermatol.2016.3601.

682 14. M. Tanaka, K. Kobiyama, T. Honda, K. Uchio-Yamada, Y. Natsume-Kitatani, K. Mizuguchi, K. Kabashima, K.
683 J. Ishii, Essential Role of CARD14 in Murine Experimental Psoriasis, *J. Immunol.* , ji1700995 (2017).

684 15. J. L. Harden, S. M. Lewis, K. C. Pierson, M. Suárez-Fariñas, T. Lentini, F. S. Ortenzio, L. C. Zaba, R.
685 Goldbach-Mansky, A. M. Bowcock, M. A. Lowes, CARD14 Expression in Dermal Endothelial Cells in Psoriasis,
686 *PLoS ONE* **9** (2014), doi:10.1371/journal.pone.0111255.

687 16. J. Bertin, L. Wang, Y. Guo, M. D. Jacobson, J.-L. Poyet, S. M. Srinivasula, S. Merriam, P. S. DiStefano, E. S.
688 Alnemri, CARD11 and CARD14 Are Novel Caspase Recruitment Domain (CARD)/Membrane-associated
689 Guanylate Kinase (MAGUK) Family Members that Interact with BCL10 and Activate NF-κB, *J. Biol. Chem.* **276**,
690 11877–11882 (2001).

691 17. J. Ruland, L. Hartjes, CARD–BCL-10–MALT1 signalling in protective and pathological immunity, *Nat. Rev.*
692 *Immunol.* , 1 (2018).

693 18. A. Howes, P. A. O'Sullivan, F. Breyer, A. Ghose, L. Cao, D. Krappmann, A. M. Bowcock, S. C. Ley, Psoriasis
694 mutations disrupt CARD14 autoinhibition promoting BCL10-MALT1-dependent NF-κB activation, *Biochem. J.*
695 **473**, 1759–1768 (2016).

696 19. M. Mellett, B. Meier, D. Mohanan, R. Schairer, P. Cheng, T. K. Satoh, B. Kiefer, C. Ospelt, S. Nobbe, M.
697 Thome, E. Contassot, L. E. French, CARD14 gain-of-function mutation alone is sufficient to drive IL-23/IL-17-
698 mediated psoriasiform skin inflammation in vivo, *J. Invest. Dermatol.* (2018), doi:10.1016/j.jid.2018.03.1525.

699 20. J. P. Sundberg, C. H. Pratt, K. A. Silva, V. E. Kennedy, W. Qin, T. M. Stearns, J. Frost, B. A. Sundberg, A. M.
700 Bowcock, Gain of function p.E138A alteration in Card14 leads to psoriasiform skin inflammation and implicates
701 genetic modifiers in disease severity, *Exp. Mol. Pathol.* **110**, 104286 (2019).

702 21. M. Wang, S. Zhang, G. Zheng, J. Huang, Z. Songyang, X. Zhao, X. Lin, Gain-of-Function Mutation of Card14
703 Leads to Spontaneous Psoriasis-like Skin Inflammation through Enhanced Keratinocyte Response to IL-17A,
704 *Immunity* **49**, 66-79.e5 (2018).

705 22. E. Van Nuffel, J. Staal, G. Baudelet, M. Haegman, Y. Driege, T. Hochepied, I. S. Afonina, R. Beyaert, MALT1
706 targeting suppresses CARD14-induced psoriatic dermatitis in mice, *EMBO Rep.* **n/a**, e49237 (2020).

707 23. T. Dainichi, R. Matsumoto, A. Mostafa, K. Kabashima, Immune Control by TRAF6-Mediated Pathways of
708 Epithelial Cells in the EIME (Epithelial Immune Microenvironment), *Front. Immunol.* **10** (2019),
709 doi:10.3389/fimmu.2019.01107.

710 24. L. Wang, Y. Guo, W. J. Huang, X. Ke, J. L. Poyet, G. A. Manji, S. Merriam, M. A. Glucksmann, P. S.
711 DiStefano, E. S. Alnemri, J. Bertin, Card10 is a novel caspase recruitment domain/membrane-associated guanylate
712 kinase family member that interacts with BCL10 and activates NF-kappa B, *J. Biol. Chem.* **276**, 21405–21409
713 (2001).

714 25. I. S. Afonina, E. Van Nuffel, G. Baudelet, Y. Driege, M. Kreike, J. Staal, R. Beyaert, The paracaspase MALT1
715 mediates CARD14-induced signaling in keratinocytes, *EMBO Rep.* **17**, 914–927 (2016).

716 26. A. Schmitt, P. Grondona, T. Maier, M. Brändle, C. Schönfeld, G. Jäger, C. Kosnopfel, F. C. Eberle, B. Schittek,
717 K. Schulze-Osthoff, A. S. Yazdi, S. Hailfinger, MALT1 Protease Activity Controls the Expression of Inflammatory
718 Genes in Keratinocytes upon Zymosan Stimulation, *J. Invest. Dermatol.* **136**, 788–797 (2016).

719 27. M. Rosenbaum, A. Gewies, K. Pechloff, C. Heuser, T. Engleitner, T. Gehring, L. Hartjes, S. Krebs, D.
720 Krappmann, M. Kriegsmann, W. Weichert, R. Rad, C. Kurts, J. Ruland, Bcl10-controlled Malt1 paracaspase activity
721 is key for the immune suppressive function of regulatory T cells, *Nat. Commun.* **10**, 2352 (2019).

722 28. H. R. Dassule, P. Lewis, M. Bei, R. Maas, A. P. McMahon, Sonic hedgehog regulates growth and
723 morphogenesis of the tooth, *Development* **127**, 4775–4785 (2000).

724 29. L. van der Fits, S. Mourits, J. S. A. Voerman, M. Kant, L. Boon, J. D. Laman, F. Cornelissen, A.-M. Mus, E.
725 Florencia, E. P. Prens, E. Lubberts, Imiquimod-Induced Psoriasis-Like Skin Inflammation in Mice Is Mediated via
726 the IL-23/IL-17 Axis, *J. Immunol.* **182**, 5836–5845 (2009).

727 30. M. Blonska, B. P. Pappu, R. Matsumoto, H. Li, B. Su, D. Wang, X. Lin, The CARMA1-Bcl10 Signaling
728 Complex Selectively Regulates JNK2 Kinase in the T Cell Receptor-Signaling Pathway, *Immunity* **26**, 55–66
729 (2007).

730 31. S. A. Watt, K. J. Purdie, N. Y. den Breems, M. Dimon, S. T. Arron, A. T. McHugh, D. J. Xue, J. H. S. Dayal, C.
731 M. Proby, C. A. Harwood, I. M. Leigh, A. P. South, Novel CARD11 Mutations in Human Cutaneous Squamous
732 Cell Carcinoma Lead to Aberrant NF-κB Regulation, *Am. J. Pathol.* **185**, 2354–2363 (2015).

733 32. K. Sommer, B. Guo, J. L. Pomerantz, A. D. Bandaranayake, M. E. Moreno-García, Y. L. Ovechkina, D. J.
734 Rawlings, Phosphorylation of the CARMA1 Linker Controls NF-κB Activation, *Immunity* **23**, 561–574 (2005).

735 33. B. S. Baker, L. Brent, H. Valdimarsson, A. V. Powles, L. Al-Imara, M. Walker, L. Fry, Is epidermal cell
736 proliferation in psoriatic skin grafts on nude mice driven by T-cell derived cytokines?, *Br. J. Dermatol.* **126**, 105–
737 110.

738 34. S. P. Singh, H. H. Zhang, J. F. Foley, M. N. Hedrick, J. M. Farber, Human T Cells That Are Able to Produce IL-
739 17 Express the Chemokine Receptor CCR6, *J. Immunol.* **180**, 214–221 (2008).

740 35. Z. Hao, K. Rajewsky, Homeostasis of peripheral B cells in the absence of B cell influx from the bone marrow, *J.*
741 *Exp. Med.* **194**, 1151–1164 (2001).

742 36. P. Wong, P. A. Coulombe, Loss of keratin 6 (K6) proteins reveals a function for intermediate filaments during
743 wound repair, *J. Cell Biol.* **163**, 327–337 (2003).

744 37. R. D. Paladini, K. Takahashi, N. S. Bravo, P. A. Coulombe, Onset of re-epithelialization after skin injury
745 correlates with a reorganization of keratin filaments in wound edge keratinocytes: defining a potential role for
746 keratin 16., *J. Cell Biol.* **132**, 381–397 (1996).

747 38. M. A. Lowes, M. Suárez-Fariñas, J. G. Krueger, Immunology of Psoriasis, *Annu. Rev. Immunol.* **32**, 227–255
748 (2014).

749 39. J. Ruland, G. S. Duncan, A. Elia, I. del Barco Barrantes, L. Nguyen, S. Plyte, D. G. Millar, D. Bouchard, A.
750 Wakeham, P. S. Ohashi, T. W. Mak, Bcl10 Is a Positive Regulator of Antigen Receptor–Induced Activation of NF-κ
751 B and Neural Tube Closure, *Cell* **104**, 33–42 (2001).

752 40. J. Ruland, G. S. Duncan, A. Wakeham, T. W. Mak, Differential Requirement for Malt1 in T and B Cell Antigen
753 Receptor Signaling, *Immunity* **19**, 749–758 (2003).

754 41. L. C. Tsoi, S. L. Spain, E. Ellinghaus, P. E. Stuart, F. Capon, J. Knight, T. Tejasvi, H. M. Kang, M. H. Allen, S.
755 Lambert, S. Stoll, S. Weidinger, J. E. Gudjonsson, S. Koks, K. Kingo, T. Esko, S. Das, A. Metspalu, M.
756 Weichenthal, C. Enerback, G. G. Krueger, J. J. Voorhees, V. Chandran, C. F. Rosen, P. Rahman, D. D. Gladman, A.
757 Reis, R. P. Nair, A. Franke, J. N. Barker, G. R. Abecasis, R. C. Trembath, J. T. Elder, Enhanced meta-analysis and
758 replication studies identify five new psoriasis susceptibility loci, *Nat. Commun.* **6**, 7001 (2015).

759 42. A. Müller, A. Hennig, S. Lorscheid, P. Grondona, K. Schulze-Osthoff, S. Hailfinger, D. Kramer, IκBζ is a key
760 transcriptional regulator of IL-36–driven psoriasis-related gene expression in keratinocytes, *Proc. Natl. Acad. Sci.*
761 **115**, 10088–10093 (2018).

762 43. A. Chiricozzi, E. Guttman-Yassky, M. Suárez-Fariñas, K. E. Nograles, S. Tian, I. Cardinale, S. Chimenti, J. G.
763 Krueger, Integrative Responses to IL-17 and TNF-α in Human Keratinocytes Account for Key Inflammatory
764 Pathogenic Circuits in Psoriasis, *J. Invest. Dermatol.* **131**, 677–687 (2011).

765 44. B. Coornaert, M. Baens, K. Heyninck, T. Bekaert, M. Haegman, J. Staal, L. Sun, Z. J. Chen, P. Marynen, R.
766 Beyaert, T cell antigen receptor stimulation induces MALT1 paracaspase–mediated cleavage of the NF-κB inhibitor
767 A20, *Nat. Immunol.* **9**, 263–271 (2008).

768 45. L. R. Klei, D. Hu, R. Panek, D. N. Alfano, R. E. Bridwell, K. M. Bailey, K. I. Oravecz-Wilson, V. J. Concel, E.
769 M. Hess, M. Van Beek, P. C. Delekta, S. Gu, S. C. Watkins, A. T. Ting, P. J. Gough, K. P. Foley, J. Bertin, L. M.
770 McAllister-Lucas, P. C. Lucas, MALT1 protease activation triggers acute disruption of endothelial barrier integrity
771 via CYLD cleavage, *Cell Rep.* **17**, 221–232 (2016).

772 46. L. Israël, M. Bardet, A. Huppertz, N. Mercado, S. Ginster, A. Unterreiner, A. Schlierf, J. F. Goetschy, H.-G.
773 Zerwes, L. Roth, F. Kolbinger, F. Bornancin, A CARD10-Dependent Tonic Signalosome Activates MALT1
774 Paracaspase and Regulates IL-17/TNF-α–Driven Keratinocyte Inflammation, *J. Invest. Dermatol.* **138**, 2075–2079
775 (2018).

776 47. S. Hailfinger, H. Nogai, C. Pelzer, M. Jaworski, K. Cabalzar, J.-E. Charton, M. Guzzardi, C. Décaillet, M. Grau,
777 B. Dörken, P. Lenz, G. Lenz, M. Thome, Malt1-dependent RelB cleavage promotes canonical NF-κB activation in
778 lymphocytes and lymphoma cell lines, *Proc. Natl. Acad. Sci. U. S. A.* **108**, 14596–14601 (2011).

779 48. T. Uehata, H. Iwasaki, A. Vandenbon, K. Matsushita, E. Hernandez-Cuellar, K. Kuniyoshi, T. Satoh, T. Mino,
780 Y. Suzuki, D. M. Standley, T. Tsujimura, H. Rakugi, Y. Isaka, O. Takeuchi, S. Akira, Malt1-Induced Cleavage of
781 Regnase-1 in CD4+ Helper T Cells Regulates Immune Activation, *Cell* **153**, 1036–1049 (2013).

782 49. H. Tanaka, Y. Arima, D. Kamimura, Y. Tanaka, N. Takahashi, T. Uehata, K. Maeda, T. Satoh, M. Murakami, S.
783 Akira, Phosphorylation-dependent Regnase-1 release from endoplasmic reticulum is critical in IL-17 response, *J.*
784 *Exp. Med.* **216**, 1431–1449 (2019).

785 50. A. Gewies, O. Gorka, H. Bergmann, K. Pechloff, F. Petermann, K. M. Jeltsch, M. Rudelius, M. Kriegsmann, W.
786 Weichert, M. Horsch, J. Beckers, W. Wurst, M. Heikenwalder, T. Korn, V. Heissmeyer, J. Ruland, Uncoupling
787 Malt1 Threshold Function from Paracaspase Activity Results in Destructive Autoimmune Inflammation, *Cell Rep.*
788 **9**, 1292–1305 (2014).

789 51. F. Schlauderer, K. Lammens, D. Nagel, M. Vincendeau, A. C. Eitelhuber, S. H. L. Verhelst, D. Kling, A.
790 Chrusciel, J. Ruland, D. Krappmann, K.-P. Hopfner, Structural analysis of phenothiazine derivatives as allosteric
791 inhibitors of the MALT1 paracaspase, *Angew. Chem. Int. Ed Engl.* **52**, 10384–10387 (2013).

792 52. D. Nagel, S. Spranger, M. Vincendeau, M. Grau, S. Raffegerst, B. Kloo, D. Hlahla, M. Neuenschwander, J.
793 Peter von Kries, K. Hadian, B. Dörken, P. Lenz, G. Lenz, D. J. Schendel, D. Krappmann, Pharmacologic Inhibition
794 of MALT1 Protease by Phenothiazines as a Therapeutic Approach for the Treatment of Aggressive ABC-DLBCL,
795 *Cancer Cell* **22**, 825–837 (2012).

53. Y.-J. Zhang, Y.-Z. Sun, X.-H. Gao, R.-Q. Qi, Integrated bioinformatic analysis of differentially expressed genes and signaling pathways in plaque psoriasis, *Mol. Med. Rep.* **20**, 225–235 (2019).

54. T. Oudot, F. Lesueur, M. Guedj, R. de Cid, S. McGinn, S. Heath, M. Foglio, B. Prum, M. Lathrop, J.-F. Prud'homme, J. Fischer, An Association Study of 22 Candidate Genes in Psoriasis Families Reveals Shared Genetic Factors with Other Autoimmune and Skin Disorders, *J. Invest. Dermatol.* **129**, 2637–2645 (2009).

55. M. Devos, D. A. Mogilenko, S. Fleury, B. Gilbert, C. Becquart, S. Quemener, H. Dehondt, P. Tougaard, B. Staels, C. Bachert, P. Vandenabeele, G. Van Loo, D. Staumont-Salle, W. Declercq, D. Dombrowicz, Keratinocyte Expression of A20/TNFAIP3 Controls Skin Inflammation Associated with Atopic Dermatitis and Psoriasis, *J. Invest. Dermatol.* **139**, 135–145 (2019).

56. S. K. Ippagunta, R. Gangwar, D. Finkelstein, P. Vogel, S. Pelletier, S. Gingras, V. Redecke, H. Häcker, Keratinocytes contribute intrinsically to psoriasis upon loss of Tnip1 function, *Proc. Natl. Acad. Sci.* **113**, E6162–E6171 (2016).

57. L. Israel, M. Mellett, Clinical and Genetic Heterogeneity of CARD14 Mutations in Psoriatic Skin Disease, *Front. Immunol.* **9** (2018), doi:10.3389/fimmu.2018.02239.

58. G. Stelzer, N. Rosen, I. Plaschkes, S. Zimmerman, M. Twik, S. Fishilevich, T. I. Stein, R. Nudel, I. Lieder, Y. Mazor, S. Kaplan, D. Dahary, D. Warshawsky, Y. Guan-Golan, A. Kohn, N. Rappaport, M. Safran, D. Lancet, The GeneCards Suite: From Gene Data Mining to Disease Genome Sequence Analyses, *Curr. Protoc. Bioinforma.* **54**, 1.30.1-1.30.33 (2016).

59. P. F. Lizzul, A. Aphale, R. Malaviya, Y. Sun, S. Masud, V. Dombrovskiy, A. B. Gottlieb, Differential Expression of Phosphorylated NF-κB/RelA in Normal and Psoriatic Epidermis and Downregulation of NF-κB in Response to Treatment with Etanercept, *J. Invest. Dermatol.* **124**, 1275–1283 (2005).

60. N. Fyhrquist, G. Muirhead, S. Prast-Nielsen, M. Jeanmougin, P. Olah, T. Skoog, G. Jules-Clement, M. Feld, M. Barrientos-Somarribas, H. Sinkko, E. H. van den Bogaard, P. L. J. M. Zeeuwen, G. Rikken, J. Schalkwijk, H. Niehues, W. Däubener, S. K. Eller, H. Alexander, D. Pennino, S. Suomela, I. Tessas, E. Lybeck, A. M. Baran, H. Darban, R. S. Gangwar, U. Gerstel, K. Jahn, P. Karisola, L. Yan, B. Hansmann, S. Katayama, S. Meller, M. Bylesjö, P. Hupé, F. Levi-Schaffer, D. Greco, A. Ranki, J. M. Schröder, J. Barker, J. Kere, S. Tsoka, A. Lauerma, V. Soumelis, F. O. Nestle, B. Homey, B. Andersson, H. Alenius, Microbe-host interplay in atopic dermatitis and psoriasis, *Nat. Commun.* **10** (2019), doi:10.1038/s41467-019-12253-y.

61. X. Liu, Q. Cai, H. Yang, Z. Gao, L. Yang, Distribution of Malassezia species on the skin of patients with psoriasis, *J. Med. Mycol.* **31**, 101111 (2021).

62. S. M. Rudramurthy, P. Honnavar, A. Chakrabarti, S. Dogra, P. Singh, S. Handa, Association of Malassezia species with psoriatic lesions, *Mycoses* **57**, 483–488 (2014).

63. Y. Sasaki, E. Derudder, E. Hobeika, R. Pelanda, M. Reth, K. Rajewsky, M. Schmidt-Supprian, Canonical NF-κB Activity, Dispensable for B Cell Development, Replaces BAFF-Receptor Signals and Promotes B Cell Proliferation upon Activation, *Immunity* **24**, 729–739 (2006).

64. K. Pechloff, J. Holch, U. Ferch, M. Schweneker, K. Brunner, M. Kremer, T. Sparwasser, L. Quintanilla-Martinez, U. Zimber-Strobl, B. Streubel, A. Gewies, C. Peschel, J. Ruland, The fusion kinase ITK-SYK mimics a T cell receptor signal and drives oncogenesis in conditional mouse models of peripheral T cell lymphoma, *J. Exp. Med.* **207**, 1031–1044 (2010).

65. C. Malosse, S. Henri, Isolation of Mouse Dendritic Cell Subsets and Macrophages from the Skin, *Methods Mol. Biol. Clifton NJ* **1423**, 129–137 (2016).

66. L. Li, Mouse epidermal keratinocyte culture, *Methods Mol. Biol. Clifton NJ* **945**, 177–191 (2013).

838 67. D. Kim, B. Langmead, S. L. Salzberg, HISAT: a fast spliced aligner with low memory requirements, *Nat.*
839 *Methods* **12**, 357–360 (2015).

840 68. M. Pertea, G. M. Pertea, C. M. Antonescu, T.-C. Chang, J. T. Mendell, S. L. Salzberg, StringTie enables
841 improved reconstruction of a transcriptome from RNA-seq reads, *Nat. Biotechnol.* **33**, 290–295 (2015).

842 69. M. I. Love, W. Huber, S. Anders, Moderated estimation of fold change and dispersion for RNA-seq data with
843 DESeq2, *Genome Biol.* **15** (2014), doi:10.1186/s13059-014-0550-8.

844 70. D. W. Huang, B. T. Sherman, R. A. Lempicki, Systematic and integrative analysis of large gene lists using
845 DAVID bioinformatics resources, *Nat. Protoc.* **4**, 44–57 (2009).

846 71. D. W. Huang, B. T. Sherman, R. A. Lempicki, Bioinformatics enrichment tools: paths toward the comprehensive
847 functional analysis of large gene lists, *Nucleic Acids Res.* **37**, 1–13 (2009).

848 72. A. Subramanian, P. Tamayo, V. K. Mootha, S. Mukherjee, B. L. Ebert, M. A. Gillette, A. Paulovich, S. L.
849 Pomeroy, T. R. Golub, E. S. Lander, J. P. Mesirov, Gene set enrichment analysis: a knowledge-based approach for
850 interpreting genome-wide expression profiles, *Proc. Natl. Acad. Sci. U. S. A.* **102**, 15545–15550 (2005).

851 73. V. K. Mootha, C. M. Lindgren, K.-F. Eriksson, A. Subramanian, S. Sihag, J. Lehar, P. Puigserver, E. Carlsson,
852 M. Ridderstråle, E. Laurila, N. Houstis, M. J. Daly, N. Patterson, J. P. Mesirov, T. R. Golub, P. Tamayo, B.
853 Spiegelman, E. S. Lander, J. N. Hirschhorn, D. Altshuler, L. C. Groop, PGC-1α-responsive genes involved in
854 oxidative phosphorylation are coordinately downregulated in human diabetes, *Nat. Genet.* **34**, 267–273 (2003).

855

ACKNOWLEDGMENTS

We would like to thank Valentin Höfl, Tanja Neumayer, Kerstin Burmeister, Nicole Prause, Olga Seelbach, Ramona Secci, Marcus Utzt, Sabrina Engels and Katharina Drobe for outstanding technical assistance, Rupert Öllinger and Roland Rad for assistance in RNA sequencing and Paul-Albert König and Kai Li for excellent discussions and comments.

Funding:

German Research Foundation (Project-ID 210592381 – SFB 1054) (JR, TK)

German Research Foundation (Project-ID 360372040 – SFB 1335) (JR, TB)

German Research Foundation (Project-ID 395357507 – SFB 1371) (JR, TB)

German Research Foundation (Project-ID 369799452 – TRR 237, RU 695/9-1) (JR)

European Research Council (ERC) under the European Union's Horizon 2020 research and innovation programme (grant agreement No 834154) (JR)

German Research Foundation (SFB TR 128) (TK)

German Research Foundation (Synergy) (TK)

German Ministry for Education and Research (KKNMS, T-B in NMO) (TK)

European Research Council (CoG 647215) (TK)

German Research Foundation (SFB 824 B10) (TB)

German Research Foundation (BI696/10-1) (TB)

Author contributions:

Conceptualization: ZK, JR

Investigation: ZK, LV, KP, LVK, TW, AM, AJ, KK, LH, EH, SM, KS and TB

Providing materials: MM, LEF and TV

Funding acquisition: TB, TK, JR

Writing – original draft: ZK, JR

Writing – review & editing: all

Competing interests: Authors declare that they have no competing interests.

DATA AND MATERIALS AVAILABILITY

The RNAseq datasets generated during this study are deposited in GEO under the association number GSEXXX. All remaining data are available in the main text or the supplementary materials. Proprietary transgenic mice are available from the corresponding author with material transfer agreement upon reasonable request.

FIGURE LEGENDS

Fig. 1. Keratinocyte-intrinsic BCL10/MALT1 signaling mediates mutant CARD14-triggered and chemically induced skin inflammation

(A) Schematics of mice with activating germline mutation in the murine *Card14* gene without (*Card14*$^{\Delta E138}$;*Bcl10*$^{KC\text{-}HET}$) or with keratinocyte-intrinsic deletion of *Bcl10* (*Card14*$^{\Delta E138}$;*Bcl10*$^{KC\text{-}KO}$).

(B-C) Ear thickness of *K14Cre* **(B)** *Card14*$^{\Delta E138}$;*Bcl10*$^{KC\text{-}HET}$, *Card14*$^{\Delta E138}$;*Bcl10*$^{KC\text{-}KO}$ and *Bcl10*$^{KC\text{-}KO}$ and **(C)** *Card14*$^{\Delta E138}$*;Malt1*$^{KC\text{-}HET}$, *Card14*$^{\Delta E138}$*;Malt1*$^{KC\text{-}KO}$ and *Malt1*$^{KC\text{-}KO}$ mice.

(D-E) Representative histological sections showing acanthotic epidermis with focal hypogranulosis and mounds of parakeratosis housing neutrophils, a few mitoses in the basal epidermis, dilated capillaries and perivascular infiltrates with lymphocytes and neutrophils in the ears of **(D**, *middle) Card14*$^{\Delta E138}$;*Bcl10*$^{KC\text{-}HET}$ and **(E**, *middle*) *Card14*$^{\Delta E138}$*;Malt1*$^{KC\text{-}HET}$ mice. No skin alterations were observed in ***(D,*** *bottom) Card14*$^{\Delta E138}$;*Bcl10*$^{KC\text{-}KO}$ and ***(E,*** *bottom) Card14*$^{\Delta E138}$*;Malt1*$^{KC\text{-}KO}$ mice and *(***D-E,** *top) K14Cre* littermate controls.

(F-G) Quantification by flow cytometry of Ly6G+CD11b+ neutrophil granulocytes from the ears of *K14Cre* **(F)** *Card14*$^{\Delta E138}$;*Bcl10*$^{KC\text{-}HET}$ and *Card14*$^{\Delta E138}$;*Bcl10*$^{KC\text{-}KO}$ and **(G)** *Card14*$^{\Delta E138}$*;Malt1*$^{KC\text{-}HET}$ and *Card14*$^{\Delta E138}$*;Malt1*$^{KC\text{-}KO}$ mice.

(H-I) Quantification by flow cytometry of TCRγ−TCRβ+ αβ T cells from the ears of *K14Cre* **(H)** *Card14*$^{\Delta E138}$;*Bcl10*$^{KC\text{-}HET}$ and *Card14*$^{\Delta E138}$;*Bcl10*$^{KC\text{-}KO}$ and **(I)** *Card14*$^{\Delta E138}$*;Malt1*$^{KC\text{-}HET}$ and *Card14*$^{\Delta E138}$*;Malt1*$^{KC\text{-}KO}$ mice.

(J-K) Quantification by flow cytometry of IL-17A+ TCRγ−TCRβ+ αβ T cells from the ears of *K14Cre* **(J)** *Card14*$^{\Delta E138}$;*Bcl10*$^{KC\text{-}HET}$ and *Card14*$^{\Delta E138}$;*Bcl10*$^{KC\text{-}KO}$ and **(K)** *Card14*$^{\Delta E138}$;*Malt1*$^{KC\text{-}HET}$ and *Card14*$^{\Delta E138}$;*Malt1*$^{KC\text{-}KO}$ mice.

(L-M) Back and ear skin thickness of *K14Cre* and *Bcl10*$^{KC\text{-}KO}$ mice before and after five days of imiquimod treatment.

(N) Quantification by flow cytometry of Ly6G+CD11b+ neutrophil granulocytes from the backs and ears of *K14Cre* and *Bcl10*$^{KC\text{-}KO}$ mice after five days of imiquimod or sham treatment.

(**O-P**) Quantification by flow cytometry of (**O**) TCRγ−TCRβ+ αβ T cells and (**P**) IL-17A+ TCRγ−TCRβ+ αβ T cells from the ears of *K14Cre* and *Bcl10*$^{KC\text{-}KO}$ mice after five days of imiquimod or sham treatment.

(**Q**) Relative mRNA expression in the back and ears of *K14Cre* and *Bcl10*$^{KC\text{-}KO}$ mice after five days of imiquimod or sham treatment.

(**R-T**) Relative mRNA expression in the ears of *K14Cre* and *Bcl10*$^{KC\text{-}KO}$ mice after five days of imiquimod or sham treatment.

Each data point represents **(B-C, F-K, L-M, O-P, R-T)** a single mouse or **(N, Q)** a treated organ (back or ear) of a mouse. Mean ± SD. Data are **(F-K)** representative of or **(L-T)** pooled from n=2 independent experiments. **(B-C, F-K, N-T)** Ordinary one-way ANOVA with Tukey's post hoc test or **(L-M)** 2-way ANOVA with Sidak's post hoc test. Scale bars represent 200 μm. n.s. = not significant.

Fig. 2. BCL10/MALT1 activation in keratinocytes drives psoriasiform skin inflammation

(A) Schematics of mice with conditional expression of *Card11*$^{\Delta Linker}$ cDNA from the *Rosa26* locus. In keratinocytes, where the K14 promoter drives Cre expression, Cre-mediated excision of the STOP cassette results in *Card11*$^{\Delta Linker}$ expression and thereby activation of keratinocyte BCL10/MALT1 complexes.

(B) Representative image of the ears of *Card11*$^{\Delta Linker\text{-}KC}$ mice.

(C) NF-κB luciferase reporter assay in keratinocytes isolated from *Card11*$^{\Delta Linker\text{-}KC}$ mice and *K14Cre* littermate controls that were cultured and transfected with NF-κB and control luciferase reporter plasmids.

(D) Relative mRNA expression in keratinocytes isolated from *Card11*$^{\Delta Linker\text{-}KC}$ mice and *K14Cre* littermate controls.

(E) Ear thickness of *Card11*$^{\Delta Linker\text{-}KC}$, *Card11*$^{\Delta Linker\text{-}KC}$*;Bcl10*$^{KC\text{-}KO}$ and *Card11*$^{\Delta Linker\text{-}KC}$*;Malt1*$^{KC\text{-}KO}$ mice and *K14Cre* littermate controls.

(F) Representative histological sections *(left, bottom)* showing acanthotic epidermis with hypogranulosis and slight hypokeratosis, basal mitoses in the epidermis, and perivascular infiltrate with lymphocytes and neutrophils in the ears of *Card11*$^{\Delta Linker\text{-}KC}$ mice. *(Left, top)* No skin lesions were observed in *K14Cre* littermates. Representative histological sections from the ears of *(right, top) Card11*$^{\Delta Linker\text{-}KC}$*;Bcl10*$^{KC\text{-}KO}$ and *(right, bottom) Card11*$^{\Delta Linker\text{-}KC}$*;Malt1*$^{KC\text{-}KO}$ mice showing the absence of epidermal thickening and inflammatory infiltrates.

(G) Baker's psoriasis histology scores based on the examination of the ears of *Card11*$^{\Delta Linker\text{-}KC}$ mice and *K14Cre* littermate controls.

Each data point represents a single mouse **(C-E, G**). Mean ± SD. Data are representative of n=2 **(C-D)** independent experiments. **(E)** Ordinary one-way ANOVA with Tukey's post hoc test or **(C-D)** Student's t test. Scale bars represent 200 μm.

Fig. 3. Skin inflammation mediated by keratinocyte BCL10/MALT1 shows the characteristics of human psoriasis

(A) Quantification by flow cytometry of Ly6G+CD11b+ neutrophil granulocytes from the ears of *Card11*$^{\Delta Linker\text{-}KC}$ mice and *K14Cre* littermate controls.

(B) Quantification by flow cytometry of TCRγ−TCRβ+ αβ T cells from the ears of *Card11*$^{\Delta Linker\text{-}KC}$ mice and *K14Cre* littermate controls.

(C) Quantification by flow cytometry of IL-17A+ TCRγ−TCRβ+ αβ T cells from the ears of *Card11*$^{\Delta Linker\text{-}KC}$ mice and *K14Cre* littermate controls.

(D-H) Relative mRNA expression in the ears of *Card11*$^{\Delta Linker\text{-}KC}$ mice and *K14Cre* littermate controls.

(I) Ear thickness of *Card11*$^{\Delta Linker\text{-}KC}$ mice and **(J)** quantification of Ly6G+CD11b+ neutrophil granulocytes from the ears of *Card11*$^{\Delta Linker\text{-}KC}$ mice treated with 200 µg anti-IL-17A or isotype control (IC) intraperitoneally for 14 days and *K14Cre* littermate controls.

Each data point represents a single mouse. Mean ± SD. Data are **(A-C)** pooled from n=2 independent experiments or are **(D, J)** representative of n=2 independent experiments. **(A-I)** Student's t test or **(J)** ordinary one-way ANOVA with Tukey's post hoc test. n.s. = not significant.

Fig. 4. Enforced BCL10/MALT1 signaling in keratinocytes triggers a lymphocyte-mediated pathology

(A) Representative histological section showing acanthotic epidermis with hyperkeratosis but no neutrophil granulocyte infiltration in the ear of *Card11*$^{\Delta Linker\text{-}KC}$*;Rag2*$^{-/-}$ mice. No skin alterations were observed in *K14Cre;Rag2*$^{-/-}$ littermates.

(B-C) Relative mRNA expression in the ears of *Card11*$^{\Delta Linker\text{-}KC}$ and *Card11*$^{\Delta Linker\text{-}KC}$*;Rag2*$^{-/-}$ mice and *K14Cre* and *K14Cre;Rag2*$^{-/-}$ littermate controls.

(D) Ear thickness in *Card11*$^{\Delta Linker\text{-}KC}$ and *Card11*$^{\Delta Linker\text{-}KC}$*;Rag2*$^{-/-}$ mice and *K14Cre* and *K14Cre;Rag2*$^{-/-}$ littermate controls.

(E) Quantification by flow cytometry of Ly6G+CD11b+ neutrophil granulocytes from the ears of *Card11*$^{\Delta Linker\text{-}KC}$ and *Card11*$^{\Delta Linker\text{-}KC}$*;Rag2*$^{-/-}$ mice and *K14Cre* and *K14Cre;Rag2*$^{-/-}$ littermate controls.

Each data point represents a single mouse. Mean ± SD. Data are representative of n=2 **(B-E)** independent experiments. **(B)** Student's t test or **(C-E)** ordinary one-way ANOVA with a Tukey post hoc test. Scale bar indicates 200 µm. n.s. = not significant.

Fig. 5. BCL10/MALT1 signaling in keratinocytes amplifies secondary cytokine circuits

(A) Keratinocytes were isolated from newborn *Bcl10*$^{+/-}$ and *Bcl10*$^{-/-}$ mice, cultured and stimulated with the indicated cytokine for 5 hours.

(B-I) (B-D, F-H) Relative mRNA expression and **(E, I)** cytokine secretion in keratinocytes isolated from **(B-E)** *Bcl10*$^{+/-}$ and *Bcl10*$^{-/-}$ **(F-I)** or *Malt1*$^{+/-}$ and *Malt1*$^{-/-}$ mice and stimulated for 5 hours with the indicated cytokines.

(J) Western blotting of normal human epidermal keratinocytes treated with siRNAs against *BCL10* or *GFP* for 72 hours (*GFP* served as a control).

(K) Relative mRNA expression in normal human epidermal keratinocytes treated with siRNAs against *BCL10* or *GFP* for 72 hours and stimulated with IL-17A for 5 hours.

(**L-M**) Relative mRNA expression in normal human epidermal keratinocytes treated with siRNAs against *CARD14* or *GAPDH* for 72 hours and stimulated with IL-17A for 5 hours (*GAPDH* served as a control).

(B-I) Each data point represents a single mouse. Mean ± SD. 2-way ANOVA with Sidak's post hoc test. (**B-I, L-M**) The data are representative of n=2 independent experiments. **(J-K)** Data are representative of n=3 independent experiments.

Fig. 6. BCL10/MALT1 signalosomes in keratinocytes inhibit specific negative regulators of inflammation

(A-D, G-K) Western blotting of keratinocytes isolated from **(A, C-D, G, J)** *Bcl10*$^{+/-}$ and *Bcl10*$^{-/-}$, **(B, H, K)** *Malt1*$^{+/-}$ and *Malt1*$^{-/-}$ or **(I)** *K14Cre* and *Card11*$^{\Delta Linker\text{-}KC}$ mice and stimulated with **(A-B, G-K)** IL-17A, **(C)** IL-1β or **(D)** TNF for the indicated time points.

(E-F) Keratinocytes were isolated from *Bcl10*$^{+/-}$ (n=2) and *Bcl10*$^{-/-}$ (n=3) mice and left unstimulated or stimulated for 5 hours with IL-17A. **(E)** Gene set enrichment analysis of the NHEK_IL17 gene set in unstimulated vs. IL17A-stimulated, *(left)* *Bcl10*$^{+/-}$ and *(right)* *Bcl10*$^{-/-}$ keratinocytes **(F)** as well as in *Bcl10*$^{+/-}$ vs. *Bcl10*$^{-/-}$ keratinocytes. The NHEK_IL17 gene set consists of genes upregulated upon IL-17A stimulation in normal human keratinocytes *(43)*.

(A-D, G-K) Data are representative of n=3 independent experiments. FL = full length, CL = cleaved, * indicates nonspecific bands.

Fig. 7. MALT1 paracaspase facilitates keratinocyte inflammatory responses by cleaving negative regulators and thus controls the magnitude of keratinocyte cytokine responses

(A) Western blotting of keratinocytes isolated from *Bcl10*$^{+/-}$ and *Bcl10*$^{-/-}$ mice and treated with siRNAs against *A20* or *GFP* for 72 hours (GFP served as a control).

(B-E) Relative mRNA expression in keratinocytes isolated from *Bcl10*$^{+/-}$ and *Bcl10*$^{-/-}$ mice and treated with siRNAs against *A20* or *GFP* for 72 hours and stimulated with IL-17A for 5 hours.

(F-H) Relative mRNA expression in keratinocytes isolated from *Malt1*$^{+/-}$ and *Malt1*$^{PM/-}$ mice and stimulated for 5 hours with IL-17A.

(I-J) (I) Ear thickness and **(J)** relative mRNA expression in the ears of *Card11*$^{\Delta Linker\text{-}KC}$*;Malt1*$^{KC\text{-}HET}$ and *Card11*$^{\Delta Linker\text{-}KC}$*;Malt1*$^{PM\text{-}KC}$ mice.

(K) Quantification by flow cytometry of Ly6G+CD11b+ neutrophil granulocytes from the ears of *Card11*$^{\Delta Linker\text{-}KC}$*;Malt1*$^{KC\text{-}HET}$ and *Card11*$^{\Delta Linker\text{-}KC}$*;Malt1*$^{PM\text{-}KC}$ mice.

Each data point represents a single mouse. Mean ± SD. (**A-H, J-K**) Data are representative of n=2 independent experiments. **(B-H)** 2-way ANOVA with Sidak's post hoc test or **(I-K)** Student's t test. FL = full length, n.s. = not significant.

Fig. 8. Keratinocyte BCL10/MALT1 signalosomes are active in sporadic human psoriasis

(A) Keratinocytes were isolated from newborn *K14Cre* and *Card11*$^{\Delta Linker\text{-}KC}$ mice, cultured and stimulated with IL-17A for 5 hours. RNAseq analysis revealed that 293 genes were significantly (log2-fold change > 1.5 and FDR < 0.05) upregulated upon BCL10/MALT1 activation. These genes were used to define the BM_activation_KC_UP gene set.

(B-C) Three transcriptomic datasets of psoriatic lesional skin and healthy donor skin were retrieved from the Gene Expression Omnibus and analyzed for *BCL10* expression.

(D-E) Two transcriptomic datasets of lesional and paired nonlesional skin of patients with sporadic psoriasis were retrieved from the Gene Expression Omnibus and analyzed for *BCL10* expression.

(F) Representative immunohistochemical staining of BCL10 in *(bottom)* lesional and *(top)* paired nonlesional skin of a patient with sporadic psoriasis.

(G) Quantification of BCL10 protein expression in lesional and paired nonlesional skin of patients with sporadic psoriasis.

(H) Enrichment plot of the BM activation_KC_UP gene set in psoriatic lesional skin vs healthy donor skin. Transcriptomic datasets of psoriatic lesional skin and healthy donor skin were retrieved from the Gene Expression Omnibus.

(I) KEGG pathways significantly enriched in differentially expressed genes (upregulated) upon BCL10/MALT1 signaling in keratinocytes isolated from *Card11*$^{\Delta Linker\text{-}KC}$ mice compared to *K14Cre* littermates. The adjusted significance of enrichment was calculated using the DAVID

online tool. KEGG pathways with black bars are significantly enriched in psoriatic lesional vs nonlesional skin *(53)*.

(J) KEGG pathways enriched in human psoriatic lesional vs nonlesional skin *(53)* are also enriched in keratinocytes isolated from *Card11*$^{\Delta Linker\text{-}KC}$ mice compared to *K14Cre* littermates. Normalized enrichment scores (NESs) were calculated using gene-set enrichment analysis.

(K) Schematic view of the role of keratinocyte BCL10/MALT1 signaling in psoriatic inflammation.

(C, E, G) Each data point represents a patient sample. Mean ± SD. **(C)** Student's t test, **(E)** paired Student's t test or **(G)** Wilcoxon one-sided, matched pairs signed rank test. Scale bars represent 100 μm. RPKM = Reads per kilobase per million mapped reads.

SUPPLEMENTARY FIGURES

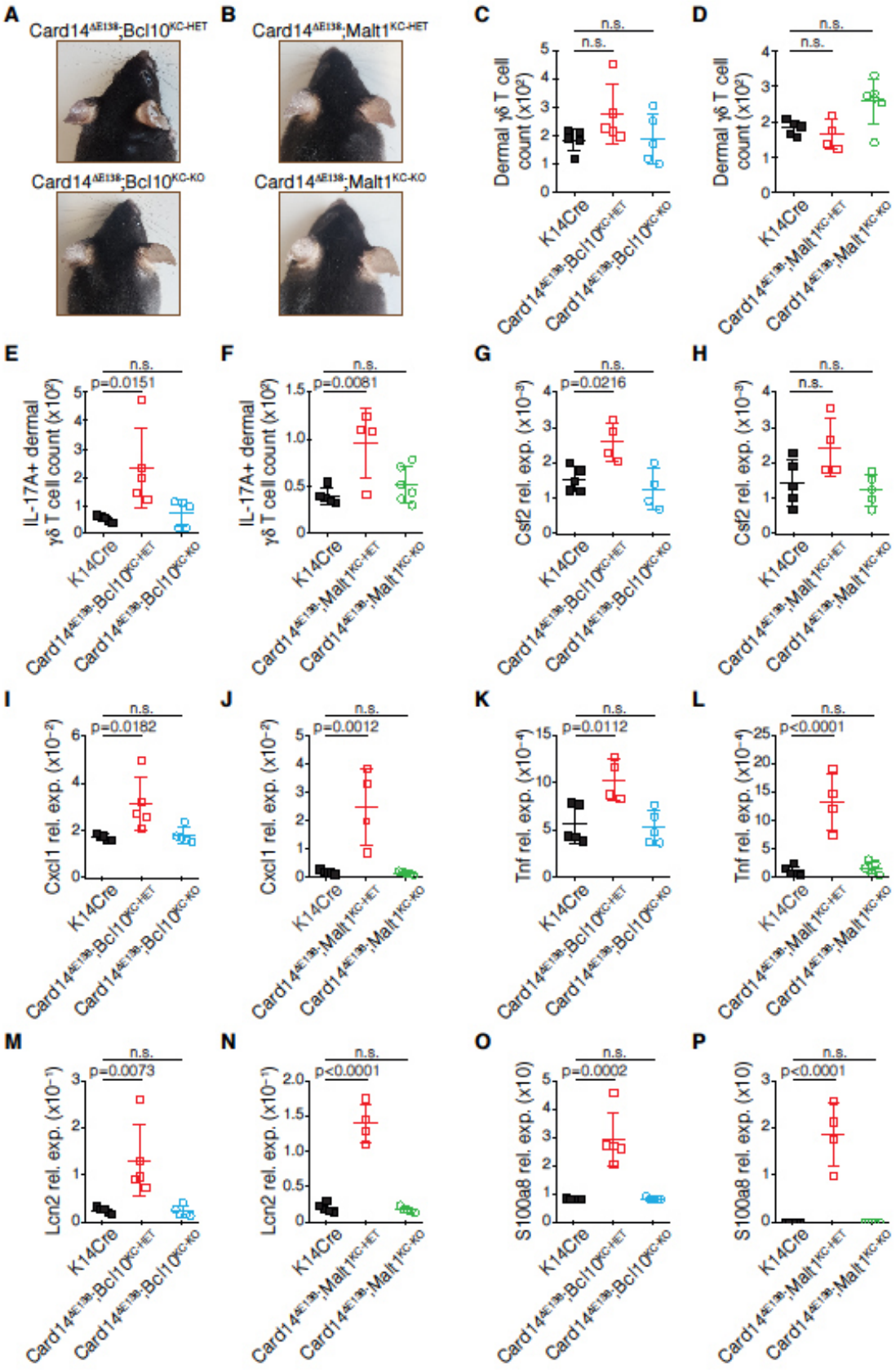
A
Card14ΔE138;Bcl10KC-HET
Card14ΔE138;Bcl10KC-KO
B
Card14ΔE138;Malt1KC-HET
Card14ΔE138;Malt1KC-KO
C
Dermal γδ T cell count (x10²)
n.s.
n.s.
D
Dermal γδ T cell count (x10²)
n.s.
n.s.
E
IL-17A+ dermal γδ T cell count (x10²)
n.s.
p=0.0151
F
IL-17A+ dermal γδ T cell count (x10²)
n.s.
p=0.0081
G
Csf2 rel. exp. (x10⁻³)
n.s.
p=0.0216
H
Csf2 rel. exp. (x10⁻³)
n.s.
n.s.
I
Cxcl1 rel. exp. (x10⁻²)
n.s.
p=0.0182
J
Cxcl1 rel. exp. (x10⁻²)
n.s.
p=0.0012
K
Tnf rel. exp. (x10⁻⁴)
n.s.
p=0.0112
L
Tnf rel. exp. (x10⁻⁴)
n.s.
p<0.0001
M
Lcn2 rel. exp. (x10⁻¹)
n.s.
p=0.0073
N
Lcn2 rel. exp. (x10⁻¹)
n.s.
p<0.0001
O
S100a8 rel. exp. (x10)
n.s.
p=0.0002
P
S100a8 rel. exp. (x10)
n.s.
p<0.0001
K14Cre
Card14ΔE138;Bcl10KC-HET
Card14ΔE138;Bcl10KC-KO
Card14ΔE138;Malt1KC-HET
Card14ΔE138;Malt1KC-KO

3

Fig. S1. Keratinocyte-intrinsic BCL10/MALT1 signaling mediates mutant CARD14-triggered skin inflammation

(A-B) Representative images of the ears of **(A)** *Card14$^{\Delta E138}$;Bcl10$^{KC\text{-}KO}$* mice and *K14Cre* and *Card14$^{\Delta E138}$;Bcl10$^{KC\text{-}HET}$* littermate controls and **(B)** *Card14$^{\Delta E138}$;Malt1$^{KC\text{-}KO}$* mice and *K14Cre* and *Card14$^{\Delta E138}$;Malt1$^{KC\text{-}HET}$* littermate controls.

(C-D) Quantification by flow cytometry of TCRγ^{med}TCRβ− dermal γδ T cells from the ears of **(C)** *Card14$^{\Delta E138}$;Bcl10$^{KC\text{-}KO}$* mice and *K14Cre* and *Card14$^{\Delta E138}$;Bcl10$^{KC\text{-}HET}$* littermate controls and **(D)** *Card14$^{\Delta E138}$;Malt1$^{KC\text{-}KO}$* mice and *K14Cre* and *Card14$^{\Delta E138}$;Malt1$^{KC\text{-}HET}$* littermate controls.

(E-F) Quantification by flow cytometry of IL-17A+ TCRγ^{med}TCRβ− dermal γδ T cells from the ears of **(E)** *Card14$^{\Delta E138}$;Bcl10$^{KC\text{-}KO}$* mice and *K14Cre* and *Card14$^{\Delta E138}$;Bcl10$^{KC\text{-}HET}$* littermate controls and **(F)** *Card14$^{\Delta E138}$;Malt1$^{KC\text{-}KO}$* mice and *K14Cre* and *Card14$^{\Delta E138}$;Malt1$^{KC\text{-}HET}$* littermate controls.

(G-P) Relative mRNA expression in the ears of **(G, I, K, M, O)** *Card14$^{\Delta E138}$;Bcl10$^{KC\text{-}KO}$* mice and *K14Cre* and *Card14$^{\Delta E138}$;Bcl10$^{KC\text{-}HET}$* littermate controls and **(H, J, L, N, P)** *Card14$^{\Delta E138}$;Malt1$^{KC\text{-}KO}$* mice and *K14Cre* and *Card14$^{\Delta E138}$;Malt1$^{KC\text{-}HET}$* littermate controls.

Each data point represents a single mouse. Mean ± SD. Data are representative of n=2 independent experiments. Ordinary one-way ANOVA with a Tukey post hoc test n.s. = not significant.

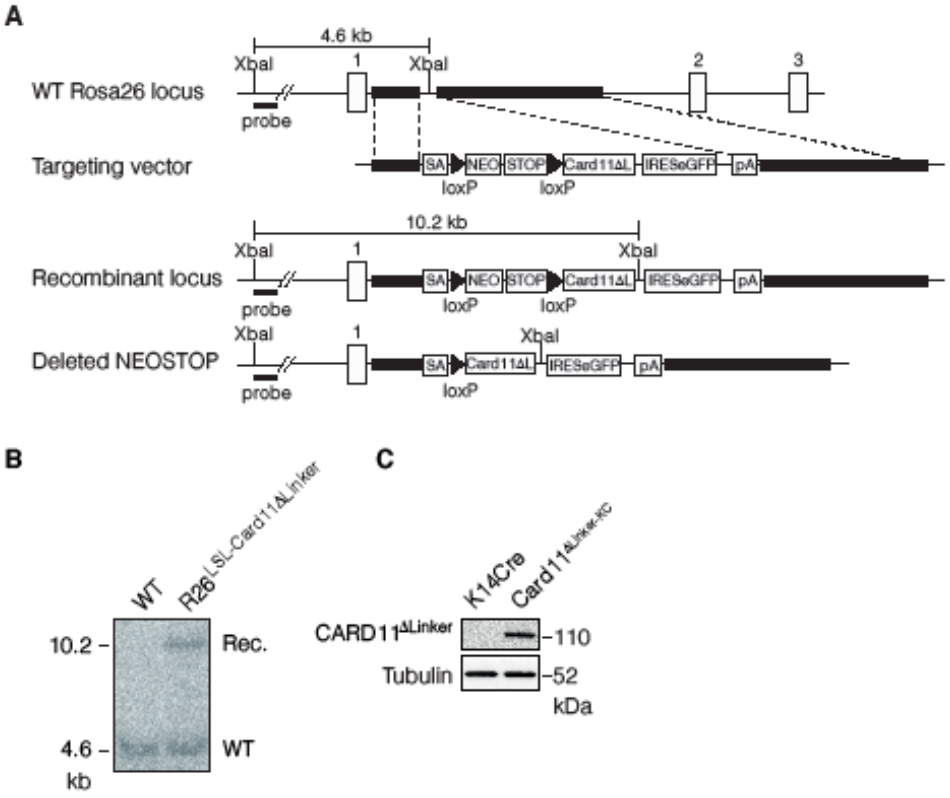
A
4.6 kb
XbaI
1
XbaI
2
3
WT Rosa26 locus
probe
Targeting vector
SA
NEO
STOP
Card11ΔL
IRESeGFP
pA
loxP
loxP
10.2 kb
XbaI
1
XbaI
Recombinant locus
probe
loxP
loxP
XbaI
1
XbaI
Deleted NEOSTOP
probe
loxP
B
WT
R26L-SL-Card11ΔLinker
10.2
Rec.
4.6
kb
WT
C
K14Cre
Card11ΔLinker-KC
CARD11ΔLinker
110
Tubulin
52
kDa

Fig. S2. Generation of a mouse with conditional Card11$^{\Delta Linker}$ expression

(A) A targeting vector containing the cDNA sequence for the murine *Card11$^{\Delta Linker}$*, followed by an *IRES-eGFP* and *polyA* signal sequence and preceded by a 5'-positioned *loxP*-flanked *Neomycin-STOP* cassette, was utilized to generate *Rosa26$^{LSL\text{-}Card11\Delta Linker}$* mice. XbaI restriction sites with the respective fragment sizes in kilobases (kb) are shown; *probe* indicates the 5'-flanking probe for Southern blot analysis, (1-3) indicate *Rosa26* exons 1-3.

(B) Southern blot of XbaI-digested genomic DNA isolated from E14K embryonic stem cell clones.

(C) Western blot of keratinocytes isolated from mice with the indicated genotypes.

SA=splice acceptor site, pA=polyA signal sequence, NEOSTOP=Neomycin-STOP cassette, R26=Rosa26, LSL=loxP-STOP-loxP, WT=wild-type.

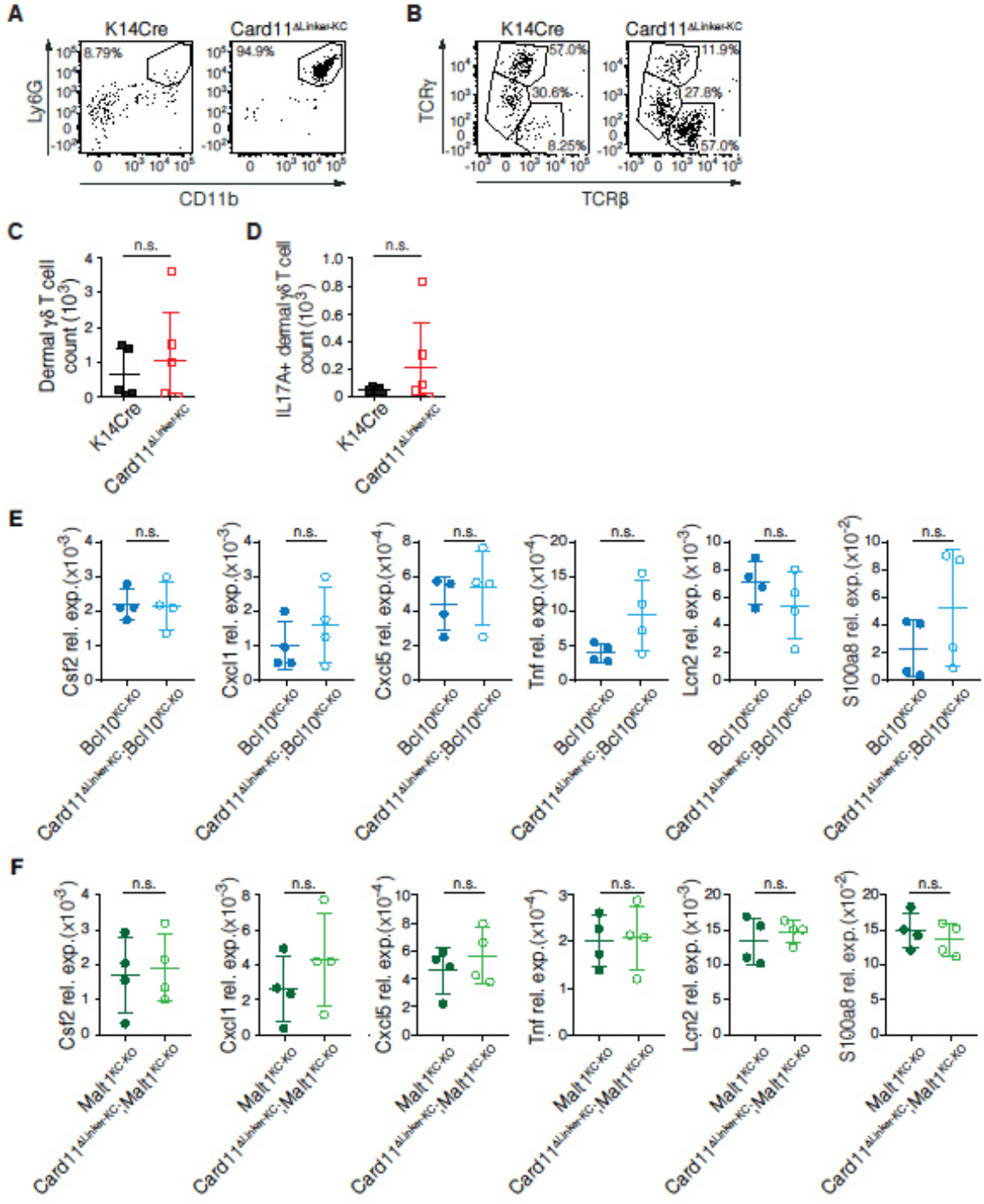
A
K14Cre
Card11ΔLinker-KC
8.79%
94.9%
Ly6G
CD11b
B
K14Cre
Card11ΔLinker-KC
57.0%
30.6%
8.25%
11.9%
27.8%
57.0%
TCRγ
TCRβ
C
n.s.
Dermal γδ T cell count (10³)
K14Cre
Card11ΔLinker-KC
D
n.s.
IL17A+ dermal γδ T cell count (10³)
K14Cre
Card11ΔLinker-KC
E
n.s.
Csf2 rel. exp.(x10⁻³)
Cxcl1 rel. exp.(x10⁻³)
Cxcl5 rel. exp.(x10⁻⁴)
Tnf rel. exp.(x10⁻⁴)
Lcn2 rel. exp.(x10⁻³)
S100a8 rel. exp.(x10⁻²)
Bcl10KC-KO
Card11ΔLinker-KC;Bcl10KC-KO
F
n.s.
Csf2 rel. exp.(x10⁻³)
Cxcl1 rel. exp.(x10⁻³)
Cxcl5 rel. exp.(x10⁻⁴)
Tnf rel. exp.(x10⁻⁴)
Lcn2 rel. exp.(x10⁻³)
S100a8 rel. exp.(x10⁻²)
Malt1KC-KO
Card11ΔLinker-KC;Malt1KC-KO

Fig. S3. BCL10/MALT1 activation in keratinocytes drives psoriasiform skin inflammation

(A) Representative flow cytometry results for live CD45+ cells isolated from the ears of *Card11*$^{\Delta Linker\text{-}KC}$ mice and *K14Cre* littermate controls. Gated on Ly6G+CD11b+ neutrophil granulocytes.

(B) Representative flow cytometry results for live CD45+CD3+ T cells isolated from the ears of *Card11*$^{\Delta Linker\text{-}KC}$ mice and *K14Cre* littermate controls. Gated on TCRγ^{high}TCRβ− dendritic epithelial T cells, TCRγ^{med}TCRβ− dermal γδ T cells and TCRγ−TCRβ+ αβ T cells.

(C) Quantification by flow cytometry of TCRγ^{med}TCRβ− dermal γδ T cells from the ears of *Card11*$^{\Delta Linker\text{-}KC}$ mice and *K14Cre* littermate controls.

(D) Quantification by flow cytometry of IL-17A+ TCRγ^{med}TCRβ− dermal γδ T cells from the ears of *Card11*$^{\Delta Linker\text{-}KC}$ mice and *K14Cre* littermate controls.

(E-F) Relative mRNA expression in the ears of **(E)** *Card11*$^{\Delta Linker\text{-}KC}$*;Bcl10*$^{KC\text{-}KO}$ mice and *Bcl10*$^{KC\text{-}KO}$ littermate controls and **(F)** *Card11*$^{\Delta Linker\text{-}KC}$*;Malt1*$^{KC\text{-}KO}$ mice and *Malt1*$^{KC\text{-}KO}$ littermate controls.

Each data point represents a single mouse. Mean ± SD. Data are representative of n=2 independent experiments. Student's t test. n.s. = not significant.

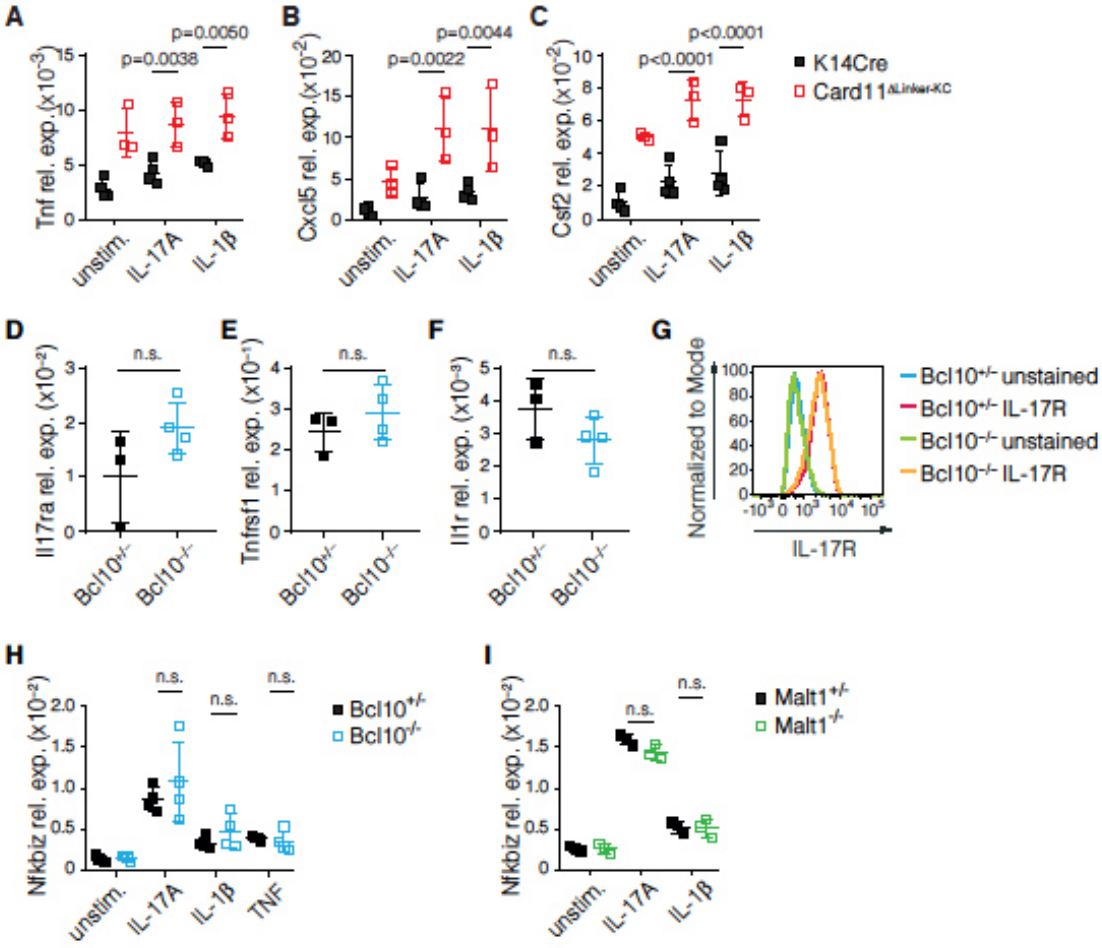
A
B
C
p=0.0050
p=0.0038
p=0.0044
p=0.0022
p<0.0001
p<0.0001
Tnf rel. exp.(x10-3)
Cxcl5 rel. exp.(x10-2)
Csf2 rel. exp.(x10-2)
unstim.
IL-17A
IL-1β
K14Cre
Card11ΔLinker-KC
D
E
F
G
n.s.
Il17ra rel. exp. (x10-2)
Tnfrsf1 rel. exp. (x10-1)
Il1r rel. exp. (x10-3)
Bcl10+/-
Bcl10-/-
Normalized to Mode
IL-17R
Bcl10+/- unstained
Bcl10+/- IL-17R
Bcl10-/- unstained
Bcl10-/- IL-17R
H
I
Nfkbiz rel. exp. (x10-2)
TNF
Malt1+/-
Malt1-/-

Fig. S4. BCL10/MALT1 signaling in keratinocytes amplifies secondary cytokine circuits

(A-C) Relative mRNA expression in keratinocytes isolated from *K14Cre* and *Card11*$^{\Delta Linker\text{-}KC}$, mice cultured and stimulated for 5 hours with the indicated cytokines.

(D-F) Relative mRNA expression in keratinocytes isolated from *Bcl10*$^{+/-}$ and *Bcl10*$^{-/-}$ mice

(G) Mean fluorescence intensity by flow cytometry in keratinocytes isolated from *Bcl10*$^{+/-}$ and *Bcl10*$^{-/-}$ mice

(H-I) Relative mRNA expression in keratinocytes isolated from **(H)** *Bcl10*$^{+/-}$ and *Bcl10*$^{-/-}$ **(I)** or *Malt1*$^{+/-}$ and *Malt1*$^{-/-}$ mice cultured and stimulated for 5 hours with the indicated cytokines.

(**A-F, H-I**) Each data point represents a single mouse. Mean ± SD. The data are representative of n=2 independent experiments. (**A-C, H-I**) 2-way ANOVA with Sidak's post hoc test and (**D-F**) Student's t-test. N.s.= not significant.

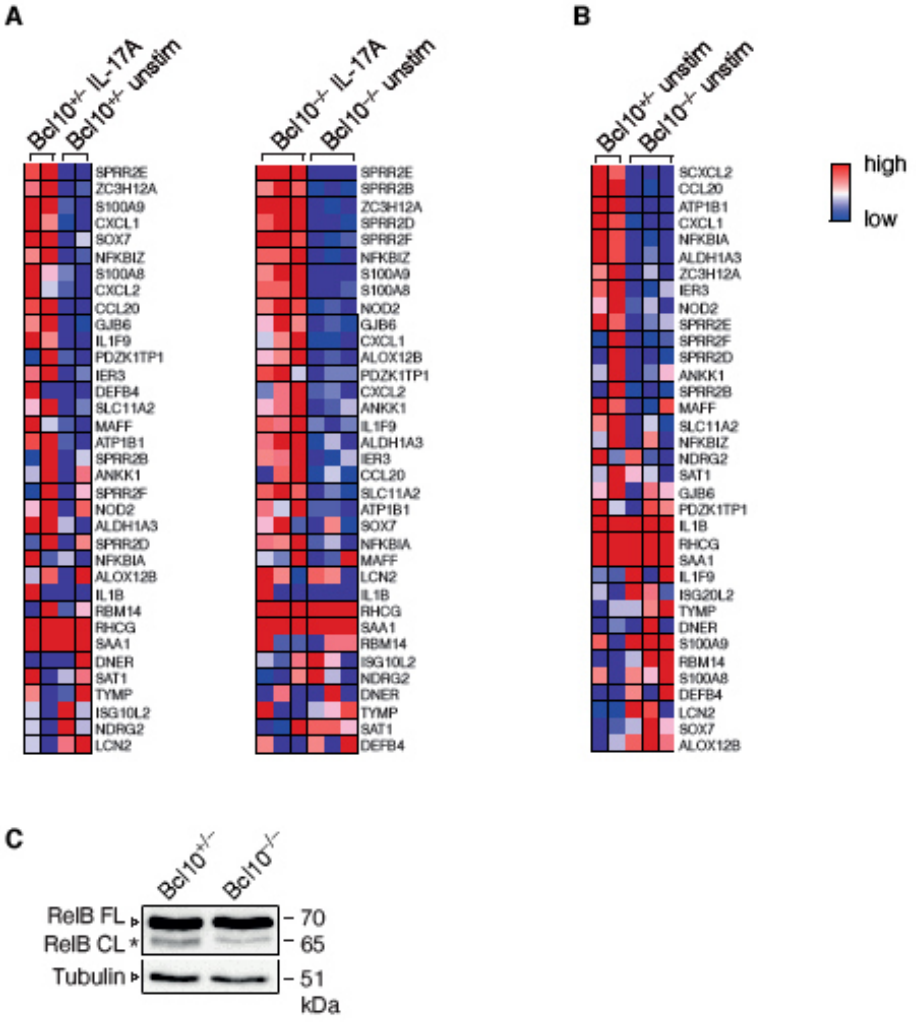
A
Bcl10+/- IL-17A
Bcl10+/- unstim
Bcl10+/- IL-17A
Bcl10-/- unstim
SPRR2E
ZC3H12A
S100A9
CXCL1
SOX7
NFKBIZ
S100A8
CXCL2
CCL20
GJB6
IL1F9
PDZK1TP1
IER3
DEFB4
SLC11A2
MAFF
ATP1B1
SPRR2B
ANKK1
SPRR2F
NOD2
ALDH1A3
SPRR2D
NFKBIA
ALOX12B
IL1B
RBM14
RHCG
SAA1
DNER
SAT1
TYMP
ISG10L2
NDRG2
LCN2
SPRR2E
SPRR2B
ZC3H12A
SPRR2D
SPRR2F
NFKBIZ
S100A9
S100A8
NOD2
GJB6
CXCL1
ALOX12B
PDZK1TP1
CXCL2
ANKK1
IL1F9
ALDH1A3
IER3
CCL20
SLC11A2
ATP1B1
SOX7
NFKBIA
MAFF
LCN2
IL1B
RHCG
SAA1
RBM14
ISG10L2
NDRG2
DNER
TYMP
SAT1
DEFB4
B
Bcl10+/- unstim
Bcl10-/- unstim
high
low
SCXCL2
CCL20
ATP1B1
CXCL1
NFKBIA
ALDH1A3
ZC3H12A
IER3
NOD2
SPRR2E
SPRR2F
SPRR2D
ANKK1
SPRR2B
MAFF
SLC11A2
NFKBIZ
NDRG2
SAT1
GJB6
PDZK1TP1
IL1B
RHCG
SAA1
IL1F9
ISG20L2
TYMP
DNER
S100A9
RBM14
S100A8
DEFB4
LCN2
SOX7
ALOX12B
C
Bcl10+/-
Bcl10-/-
RelB FL
RelB CL *
Tubulin
70
65
51
kDa

Fig. S5. BCL10/MALT1 signalosomes in keratinocytes inhibit specific negative regulators of inflammation

(A-B) Heat map of the NHEK_IL17 gene set in (**A**) unstimulated vs. IL17A-stimulated, *(left)* *Bcl10*$^{+/-}$ and *(right)* *Bcl10*$^{-/-}$ keratinocytes (**B**) as well as in *Bcl10*$^{+/-}$ vs. *Bcl10*$^{-/-}$ keratinocytes. The NHEK_IL17 gene set consists of genes upregulated upon IL-17A stimulation in normal human keratinocytes (*1*).

(**C**) Western blotting of keratinocytes isolated from *Bcl10*$^{+/-}$ vs. *Bcl10*$^{-/-}$ mice. Data are representative of n=2 independent experiments. FL = full length, CL = cleaved.

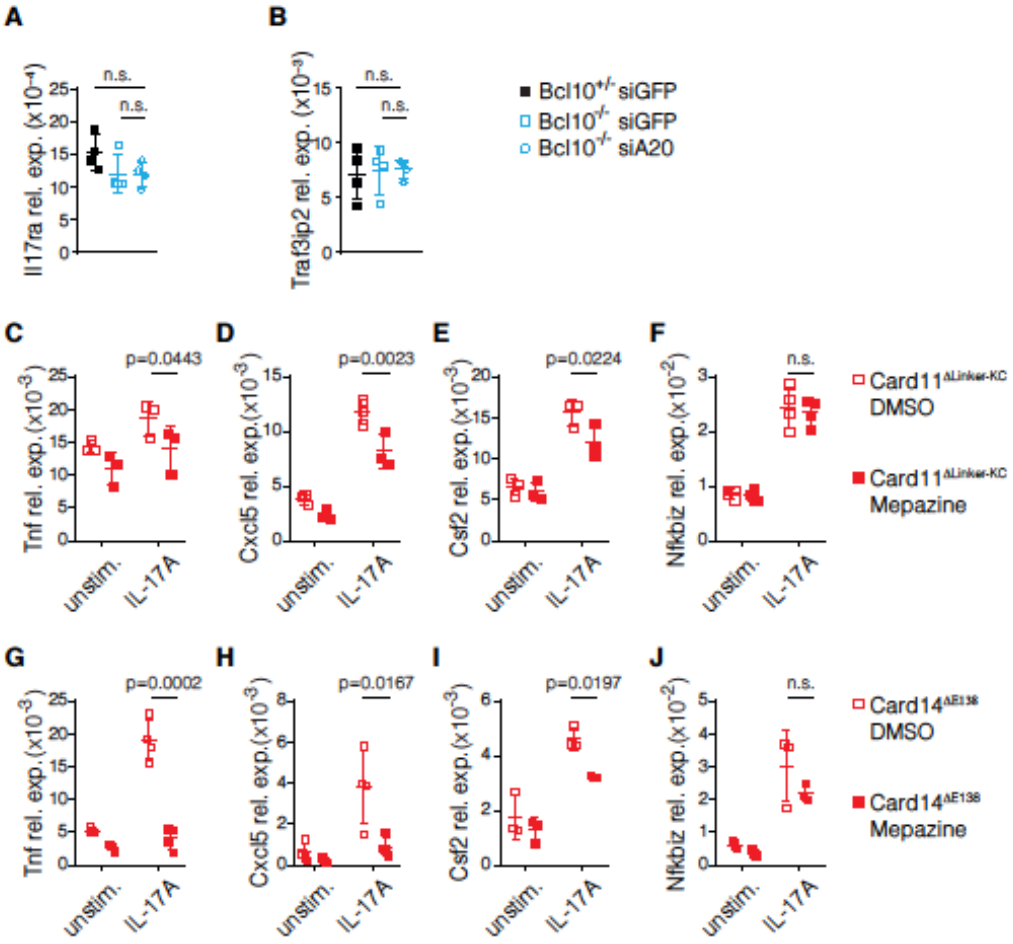
A
B
Il17ra rel. exp. (x10⁻⁴)
Traf3ip2 rel. exp. (x10⁻³)
n.s.
n.s.
Bcl10+/- siGFP
Bcl10-/- siGFP
Bcl10-/- siA20
C
D
E
F
Tnf rel. exp. (x10⁻³)
Cxcl5 rel. exp.(x10⁻³)
Csf2 rel. exp. (x10⁻³)
Nfkbiz rel. exp.(x10⁻²)
p=0.0443
p=0.0023
p=0.0224
unstim.
IL-17A
Card11ΔLinker-KC DMSO
Card11ΔLinker-KC Mepazine
G
H
I
J
p=0.0002
p=0.0167
p=0.0197
Card14ΔE138 DMSO
Card14ΔE138 Mepazine

Fig. S6. MALT1 paracaspase facilitates keratinocyte inflammatory responses by cleaving negative regulators and thus controls the magnitude of keratinocyte cytokine responses

(**A-B**) Relative mRNA expression in keratinocytes isolated from *Bcl10*$^{+/-}$ and *Bcl10*$^{-/-}$ mice and treated with siRNAs against *A20* or *GFP* for 72 hours and stimulated with IL-17A for 5 hours.

(C-J) Relative mRNA expression in keratinocytes isolated from (**C-F**) *Card11*$^{\Delta Linker\text{-}KC}$ or (**G-J**) *Card14*$^{\Delta E138}$ mice, cultured and treated with mepazine or DMSO as a control for 6 hours and stimulated with IL-17A for 5 hours.

Each data point represents a single mouse. Mean ± SD. The data are representative of n=2 independent experiments. 2-way ANOVA with Sidak's post hoc test.

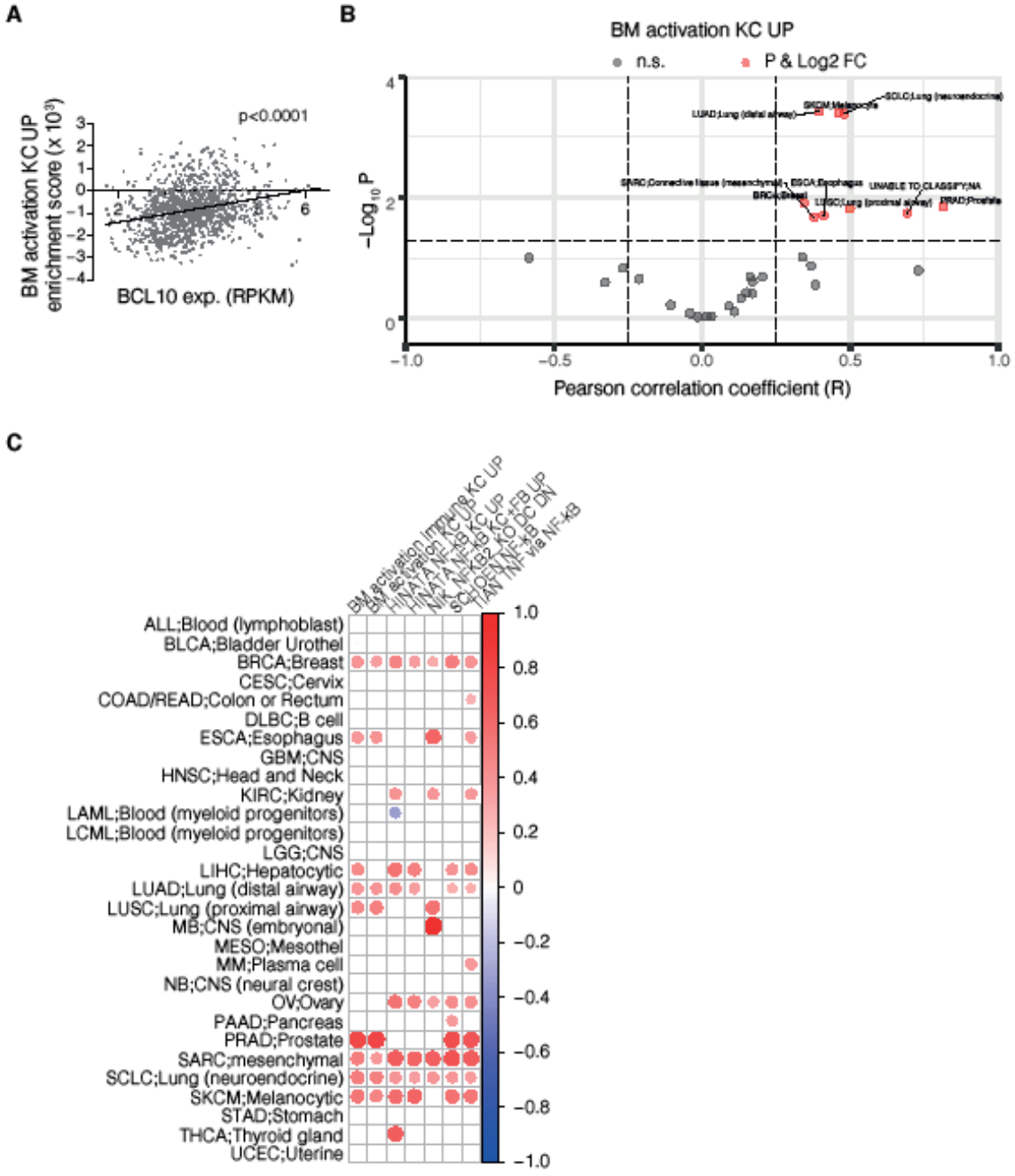
A
p<0.0001
BM activation KC UP enrichment score (x 10^3)
BCL10 exp. (RPKM)
B
BM activation KC UP
n.s.
P & Log2 FC
−Log10 P
Pearson correlation coefficient (R)
C
BM activation immune KC UP
BM activation KC UP
HINATA NF-kB KC UP
HINATA NF-kB KC FB UP
NIK NFKB2 KO FC DN
SCHUETZ NF-kB
TIAN TNF via NF-kB
ALL;Blood (lymphoblast)
BLCA;Bladder Urothel
BRCA;Breast
CESC;Cervix
COAD/READ;Colon or Rectum
DLBC;B cell
ESCA;Esophagus
GBM;CNS
HNSC;Head and Neck
KIRC;Kidney
LAML;Blood (myeloid progenitors)
LCML;Blood (myeloid progenitors)
LGG;CNS
LIHC;Hepatocytic
LUAD;Lung (distal airway)
LUSC;Lung (proximal airway)
MB;CNS (embryonal)
MESO;Mesothel
MM;Plasma cell
NB;CNS (neural crest)
OV;Ovary
PAAD;Pancreas
PRAD;Prostate
SARC;mesenchymal
SCLC;Lung (neuroendocrine)
SKCM;Melanocytic
STAD;Stomach
THCA;Thyroid gland
UCEC;Uterine

Fig. S7. *BCL10* expression correlates with the transcriptomic changes induced by activation of BCL10/MALT1 signalosomes

(A-B) Correlation of *BCL10* RNA expression and enrichment score of the BM_activation_KC_UP gene set in ca. 800 annotated CCLE cell lines, **(B)** stratified according to tissue of origin.

(C) Correlation of *BCL10* RNA expression and enrichment score of the indicated gene sets in ca. 800 annotated CCLE cell lines, stratified according to tissue of origin. The color and size of the circles correspond to the correlation coefficient between *BCL10* expression and the enrichment score of the respective gene set. Only significant correlations are presented.

Each data point represents **(A)** a cell line or **(B)** a group of cell lines with the same tcga code, i.e., tissue of origin. **(A-C)** The enrichment score was calculated using single sample gene set enrichment analysis. Pearson's linear regression was used to calculate the significance of correlations. RPKM = Reads per kilo base per million mapped reads.

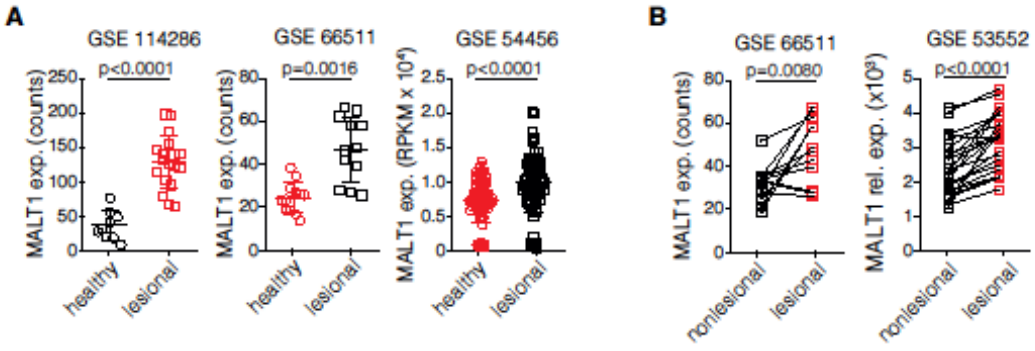
A
GSE 114286
p<0.0001
MALT1 exp. (counts)
healthy
lesional
GSE 66511
p=0.0016
MALT1 exp. (counts)
healthy
lesional
GSE 54456
p<0.0001
MALT1 exp. (RPKM x 10⁴)
healthy
lesional
B
GSE 66511
p=0.0080
MALT1 exp. (counts)
nonlesional
lesional
GSE 53552
p<0.0001
MALT1 rel. exp. (x10⁸)
nonlesional
lesional

Fig. S8. *MALT1* expression is increased in the lesional psoriatic skin

(A) Three transcriptomic datasets of psoriatic lesional skin and healthy donor skin were retrieved from the Gene Expression Omnibus and analyzed for *MALT1* expression. RPKM = Reads per kilo base per million mapped reads.

(B) Two transcriptomic datasets of lesional and paired nonlesional skin of patients with sporadic psoriasis were retrieved from the Gene Expression Omnibus and analyzed for *MALT1* expression.

SUPPLEMENTARY TABLES

Table S1. Enriched KEGG pathways in significantly upregulated genes in *Card11*$^{\Delta Linker\text{-}KC}$ keratinocytes compared to K14Cre keratinocytes using DAVID functional annotation analysis (FDR < 25%)

ID	Term	Count	%	P Value	Genes	Fold Enrich-ment	FDR
Mmu 05168	Herpes simplex infection	22	8,15	2,52E-13	Oas1a, Oas1b, Oas1g, Oas2, Oas3, Cd74, Traf1, Ccl2, Ccl5, C3, H2-M2, H2-Q2, H2-Q7, Ifit1bl1, Ifih1, Irf7, Irf9, Ifit1, Sp100, Stat1, Stat2, Tap2	7,82	3,02E-10
Mmu 05164	Influenza A	17	6,30	7,40E-10	Oas1a, Oas1b, Oas1g, Oas2, Oas3, Mx2, Ccl2, Ccl5, Cxcl10, Ifih1, Irf7, Irf9, Pik3r5, Rsad2, Stat1, Stat2, Tnfsf10	7,35	8,86E-07
Mmu 04668	TNF signaling pathway	14	5,19	1,67E-09	Traf1, Ccl2, Ccl5, Cxcl10, Cxcl2, Cxcl3, Cx3cl1, Csf2, Ifi47, Il18r1, Mmp9, Pik3r5, Tnfrsf1b, Tnfaip3	9,50	1,99E-06
Mmu 04060	Cytokine-cytokine receptor interaction	18	6,67	1,70E-08	Cd40, Ccl2, Ccl5, Cxcl10, Cxcl11, Cxcl2, Cxcl5, Cxcl9, Cx3cl1, Csf2, Csf3, Il18r1, Il18rap, Il5ra, Tgfb2, Tnfsf10, Tnfrsf11b, Tnfrsf1b	5,50	2,04E-05
Mmu 05162	Measles	14	5,19	2,56E-08	Oas1a, Oas1b, Oas1g, Oas2, Oas3, Mx2, Ifih1, Irf7, Irf9, Pik3r5, Stat1, Stat2, Tnfsf10, Tnfaip3	7,61	3,06E-05
Mmu 05160	Hepatitis C	13	4,81	2,23E-07	Oas1a, Oas1b, Oas1g, Oas2, Oas3, Ifit1bl1, Irf1, Irf7, Irf9, Ifit1, Pik3r5, Stat1, Stat2	7,07	2,67E-04
Mmu 05133	Pertussis	8	2,96	5,43E-05	C2, Nos2, C1ra, C1s2, C1s1, C3, Irf1, Cxcl5	7,99	6,50E-02
Mmu 04620	Toll-like receptor signaling pathway	9	3,33	5,69E-05	Cxcl10, Ccl5, Cxcl11, Cxcl9, Irf5, Irf7, Pik3r5, Stat1, Cd40	6,59	6,81E-02
Mmu 04062	Chemokine signaling pathway	12	4,44	5,73E-05	Cxcl10, Stat2, Cxcl2, Ccl5, Cxcl11, Cxcl3, Cxcl9, Cx3cl1, Pik3r5, Stat1, Ccl2, Cxcl5	4,53	6,85E-02

KEGG, Kyoto Encyclopedia of Genes and Genomes